

Application of Neutron Scattering to Study Materials and Transition Processes in Lithium Energy Storage Devices at the IBR-2 Pulsed Reactor

I. A. Bobrikov^{a, b, *}, I. V. Gapon^{a, c}, and M. V. Avdeev^{a, b}

^a Frank Laboratory of Neutron Physics, Joint Institute for Nuclear Research, Dubna, Russia

^b Dubna State University, Dubna, Russia

^c Institute for Safety Problems of Nuclear Power Plants, National Academy of Sciences of Ukraine, Chornobyl, Ukraine

*e-mail: bobrikov@nf.jinr.ru

Received August 16, 2021; revised September 16, 2021; accepted September 20, 2021

Abstract—The review covers the development of thermal neutron scattering methods for studying and diagnosing components of lithium energy storage devices at the IBR-2 pulsed reactor of the Joint Institute for Nuclear Research (Dubna, Russia). Experimental structural investigations of electrode materials and electrochemical interfaces over the past ten years are summarized. Their results enable a relationship to be established between the structure of the components of the electrochemical cells and their macroscopic characteristics under different conditions and better insight to be gained into the features of physicochemical processes occurring in them, which has allowed formulating recommendations on the composition and synthesis of materials for improving the capacity and operational safety of lithium energy storage devices.

DOI: 10.1134/S1063779622030030

CONTENTS

1. INTRODUCTION	674
2. EXISTING AND PROSPECTIVE LITHIUM ENERGY STORAGE DEVICES	675
2.1. General Principles of Operation of Lithium Batteries	675
2.2. Types of Existing and Prospective Lithium Energy Storage Devices and the Corresponding Structure Issues	676
2.2.1. Lithium-ion batteries of the intercalation type	676
2.2.2. Lithium-ion batteries with a metal anode	678
2.2.3. Lithium–oxygen batteries	678
3. STRUCTURAL INVESTIGATIONS USING NEUTRON SCATTERING METHODS	678
3.1. Bragg Diffraction	678
3.2. Reflectometry	683
3.3. Small-Angle Scattering	687
4. STRUCTURAL DIAGNOSTICS	694
5. CONCLUSIONS	694

1. INTRODUCTION

Wide promotion of lithium energy storage devices that began in the mid-1990s entailed fundamental changes in the current style of life. The high energy capacity of these storage devices drives the present-day rapid development of electric transport, robotics technologies, portable electronic devices, etc. Lithium-ion batteries grow more and more common in green energy as solar and wind energy storages. The importance of this type of energy storage device was recognized by awarding the Nobel Prize in Chemistry 2019 to M. Whittingham, J. Goodenough, and A. Yoshino “for the development of lithium-ion batteries.” The use of lithium cobalt oxide as a cathode material, artificial graphite as an anode material, and lithium salts in liquid electrolytes was a revolutionary step in the development of compact energy storage devices. The lithium-ion battery is based on the ability of the electrode materials to intercalate and deintercalate lithium ions during the battery charge or discharge process. To achieve a higher energy capacity compared to intercalation-type lithium-ion energy storage devices, nonintercalation lithium storage devices are also extensively investigated, which include lithium-ion batteries with a metal anode, lithium–sulfur and lithium–oxygen cells, etc. Lithium gives rise to a few features related to its high chemical activity that have to be considered in developing and designing the cor-

responding energy storage devices. In this connection, the currently important problem is to optimize lithium batteries with allowance for physicochemical processes in their components, while their further development is dependent on the solution of the global problem of increasing their energy capacity with ensuring their operational safety.

Investigations of lithium energy storage devices are naturally connected with the studies of the electrode structure evolution and the electrochemical interfaces during the operation. In the former case, of interest are changes in the crystal structure of anode and cathode materials during the battery charge and discharge. In the latter case, the study is concerned with the neighborhood of the working surface of the electrodes, which changes due to deposition of lithium and products of its chemical interaction with the electrolyte on the surface of the electrodes. It is also of interest to reveal the causes and conditions for occurrence of structural inhomogeneities on the surface of the electrodes, which develop into nanosized and submicron formations at interfaces. In current research, the focus is on the possibility of studying how electrochemical cells function, and therefore it is topical to develop methods that allow real-time studies of the corresponding processes.

Nuclear-physics methods based on penetrating radiation, such as neutron radiation, make it possible to study various physicochemical features of lithium energy storage devices both in exploratory studies with model systems and in diagnostics of materials in real (including commercial) electrochemical devices. Scattering of thermal neutrons is extensively used in research reactors and spallation sources to gain detailed structural information concerning electrochemical lithium storage devices. Low brightness of neutron sources, as compared to synchrotron radiation (SR) sources, is compensated by specific features of neutron radiation that allow unique experiments to be conducted. Neutrons are characterized by high penetrability, which makes it possible to “view” hidden phases and interfaces in storage devices. They weakly interact with substance, which entirely eliminates chemical side effects. Unlike SR, neutrons are sensitive to light elements, especially to hydrogen and lithium. Finally, their scattering exhibits strong isotopic sensitivity, in particular to the H/D substitution. The latter ensures contrast variation of a wide range of materials by deuteration. Neutron scattering methods most actively used in structural investigations of materials for lithium batteries are diffraction, reflectometry, and small-angle scattering. To better understand specific functioning features of lithium current sources, it is necessary to develop methods for studying processes occurring in hidden volumes of the system under investigation (battery) during electrochemical reactions. In this connection it is of interest to study nonequilibrium states, which implies active use of the following modes: *ex situ* (evolution of processes

is initiated for several similar electrochemical cells and terminated at particular stages with subsequent disassembling of the cells for extraction and measurements of different components), *in situ* (evolution of processes starts in one cell and terminates for measuring the state of its components without disassembling the cell), and *operando* (evolution of processes is followed for one functioning cell in the real time in the maximum realistic state).

In the past years, a particular line of research emerged in the Frank Laboratory of Neutron Physics of the Joint Institute for Nuclear Research (FLNP, JINR, Dubna, Russia) which is aimed at developing thermal neutron scattering methods for investigation and diagnostics of components of chemical energy storage devices, including lithium current sources. This review summarizes the corresponding structural investigations of electrode materials and electrochemical interfaces performed at the IBR-2 pulsed reactor in the last ten years. These investigations fully reflect the general world electrochemistry-related trends in development of neutron scattering methods and neutron centers recently reviewed in [1–6]. First of all, the problems of the existing and prospective lithium energy storage devices and the corresponding structure issues are generally treated in Section 2. Exploratory structural studies with model systems using neutron scattering methods at the IBR-2 facilities are presented in Section 3. Examples of using the above facilities to perform structural diagnostics of materials and devices for practical applications are given in Section 4.

2. EXISTING AND PROSPECTIVE LITHIUM ENERGY STORAGE DEVICES

2.1. Working Principles of Lithium-Ion Batteries

Generally, an electric battery is a device that stores chemical energy when connected to a dc power supply. When a charged battery is connected to an external circuit, the stored energy is converted to an electric current that performs effective work. These processes are reversible and repeatable, which allows multiple charge and discharge of a battery.

Operation of rechargeable chemical current sources is based on reversible redox reactions resulting in motion of electrons and positive ions from the anode (an electrode on which ions are oxidized) to the cathode (an electrode where reduction of ions occurs) during the discharge and in the reverse direction during the charge of the battery. In practice, these reactions are induced using an intermediate component, an electrolyte, which has no electron conduction and thus allows the electron flow to be separated from the ion flow: electrons move in the external circuit, and positively charged ions needed for the reduction reaction to occur on the cathode move through the electrolyte. A liquid electrolyte is typically used with a

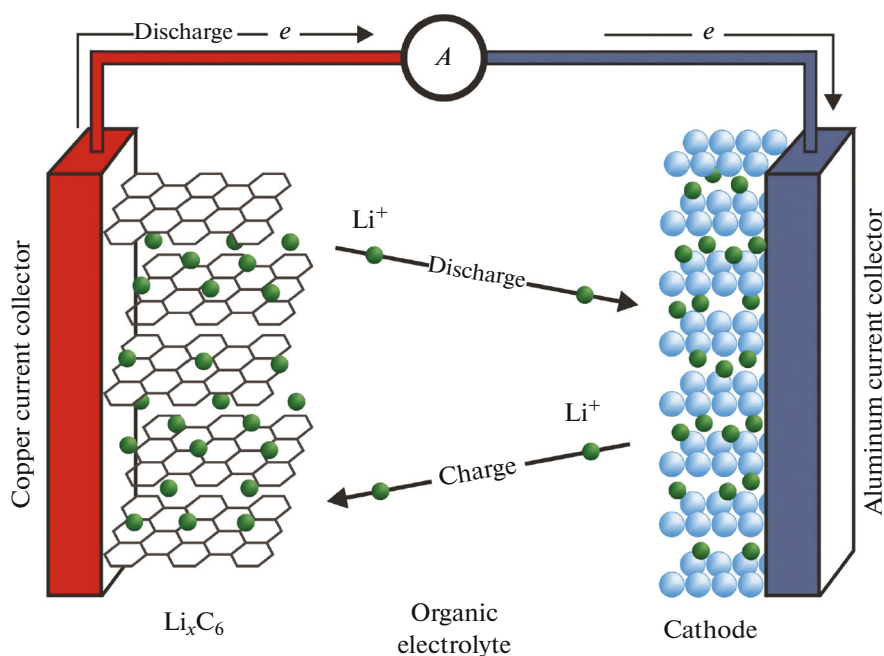


Fig. 1. Schematic principle of operation of the intercalation-type lithium-ion storage device. The figure is reproduced from [1].

separator, a porous dielectric material that separates efficiently the cathode from the anode, which prevents the short circuit. The separator is unnecessary when a solid electrolyte is used (these electrolytes have been at the development and introduction stage during the writing of the review).

Wide application of rechargeable lithium-ion batteries (LIBs) is a result of many investigations and multiparameter optimization primarily intended for increasing specific capacity (capacity per unit mass of the electrodes) and charge/discharge power (rate). Other optimized characteristics are the recharging efficiency (recovery of the initial potential after a charge/discharge cycle and transferred-to-total charge ratio), cycling (retaining of the above characteristics during multiple charge/discharge cycles), and cost and availability of the materials. Because of possible side effects, it is important to ensure safety (e.g., fire and explosion safety). Finally, when developing LIBs, one should observe ecological requirements, that is, use recyclable materials and materials with the lowest impact on the environment and living organisms.

2.2. Types of Existing and Prospective Lithium Storage Devices and the Corresponding Structure Issues

2.2.1. Lithium-ion batteries of the intercalation type. Storage devices that now best comply with the main above-mentioned requirements are those based on the reversible process of intercalation of lithium ions in the electrode material. In current lithium-ion intercalation batteries the active material of the nega-

tive electrode is graphite, and the active materials used for the positive electrode are lithium cobalt, nickel, and manganese oxides with their layered crystal structure and composites based on modified spinel (e.g., lithium manganese spinel) and olivine (lithium iron phosphate). Electrolytes for LIBs are solutions of lithium salts (usually LiClO_4 , LiPF_6 , and LiBF_4) [7] in anhydrous organic solvents, mostly various carbonate esters in combination with simple ethers.

During the battery charge lithium is extracted from the material of the positive electrode and inserted in the material of the negative electrode (Fig. 1). During the discharge the processes are reversed. The capacity diagram of different anode and cathode materials relative to the standard Li/Li^+ electrode is shown in Fig. 2. Energy storage capacity characteristics are governed first of all by the specific quantity of (de)intercalated lithium and the potential of its extraction, while the power characteristics are determined by the features of the (de)intercalation process and its accompanying structural changes in the material. These changes should be reversible. In practice, presence of irreversible or partially reversible phase transitions and reactions decreases the service life of the battery. To keep track of these reactions, it is very important to investigate the material structure and phase transitions during LIB charge/discharge. Specific intercalation capacity of carbon materials (LiC_6 is formed on the negative electrode during charging) approaches 400 mA h/g [8]. This capacity is retained in multiple cycling (losses are below 20% per 1000 cycles). Silicon and silicon-carbon composite materials are also actively studied as a substitution for

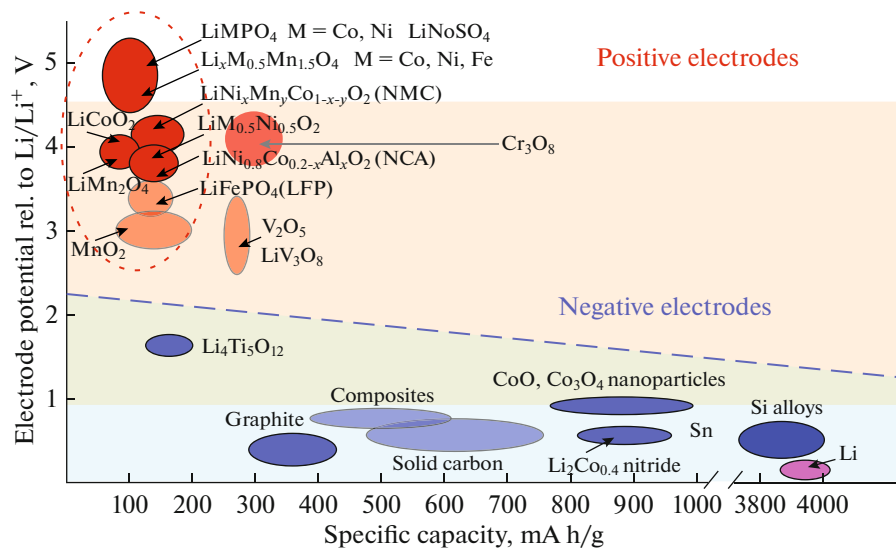


Fig. 2. Diagram of specific capacities of various materials relative to the standard Li/Li^+ electrode.

carbon ones [8]. However, the increase in the capacity of intercalation storage devices is largely limited by the capacity of positive electrode materials. Searching for and improving electrode materials that enable high specific capacitance and meet many other requirements on electrochemical storage devices are among the important directions in modern materials science.

Practical implementation of intercalation-type batteries requires wide technological optimization aimed at increasing efficiency through providing uniformity of electrochemical processes over the entire volume of the battery components. Apart from the active material, real electrodes contain additional components that ensure mechanical stability (polymeric binder) and electron conduction (e.g., carbon in cathodes). Their packing governs penetration of liquid electrolyte in materials and provides electrochemical surface (contact of electrolyte and electrode material grains). Hence follows a natural interest in nanostructured materials in which the active component has a large liquid-electrolyte-accessible contact area. Note that even a $\sim 10\%$ increase in useful characteristics of the already employed types of batteries is appreciably beneficial because of their mass-scale usage. Structural characterization of cathodes and anodes directly in the prototype batteries helps substantially reduce the time to search for optimum organization of electrodes.

In reality, (de)intercalation processes are more complicated than shown in Fig. 1 because of a number of accompanying effects. In batteries with liquid electrolytes lithium reduced on the electrode instantly reacts with the liquid electrolyte due to high electrochemical activity, which leads to partial chemical decomposition of the electrolyte. Reaction products are deposited on the electrode surface in the form of a

passivating solid electrolyte interface (SEI) layer of 10–20 Å thickness. On the one hand, the SEI layer is an ion conductor and an electron insulator. In addition, it protects the electrode material against the contact with the electrolyte, preventing further electrolyte consumption. On the other hand, the SEI is structurally and compositionally inhomogeneous, which hampers uniform transport of lithium ions, and also unstable and prone to destruction in LIB cycling, which leads to further local reaction of the electrolyte with the electrode material. This all predetermines formation of nonuniform lithium deposits (in the form of needles, dendrites, etc.), which results in reduction of current output, short circuit of opposite electrodes, excessive heat release, and a decreasing number of cells working cycles. However, ways for understanding the occurrence and development of these deposits are still obscure. The possible factors explaining this phenomenon are summarized in [9]. Now it can be said that controllable formation of SEI layers immediately in the contact region of the electrolyte and the electrode material has allowed safe and efficient usage of the lithium-ion technology. To determine the SEI composition and control SEI formation is still an ambitious objective.

The growth of dendrites and other formations in the electrolyte volume is additionally hindered by the separator. At present, safety is particularly important, and therefore lithium-ion batteries with a solid electrolyte gain widespread use. Capacity characteristics of these batteries are slightly lower, but it is appreciably difficult for nonuniform deposits to grow in a solid backing. A solid electrolyte is actually a separator with good diffuseness for lithium cations. This gave a new stimulus to development of ion-conducting solid materials.

2.2.2. Lithium-ion batteries with a metal anode. A possibility of achieving fundamentally new capacity characteristics of lithium batteries is now associated with nonintercalation sources, where negative electrodes are made of materials with a theoretically high specific capacity. It is seen in Fig. 2 that these can be metal electrodes whose atoms transfer in the form of cations to the electrolyte during discharge and are reduced on the electrode again during charging.

Naturally, the highest-capacity material for lithium battery anodes can be metallic lithium. Lithium is the lightest metal (density 0.53 g/cm^3 , $M = 6.94 \text{ g/mol}$ [10]). It also has the lowest redox potential among metals (-3.04 V relative to the standard hydrogen electrode, SHE) and specific capacity of about 3860 mA h/g [11].

A pure lithium anode gives a theoretical maximum gain up to a factor of 10 as compared to the currently employed intercalation storage devices (e.g., graphite) and allows making battery assemblies with lithium-free cathodes, which may considerably simplify the manufacture process involving some promising cathode materials (e.g., sulfur-based ones [12]).

The fundamental problem of using a pure metal, especially lithium, is intensive growth of dendrite and needle-shaped structures on the electrode surface during charging, i.e., during deposition of lithium. As in intercalation batteries, various modifications of liquid electrolytes, separators, and solid electrolytes are semiempirically tried out for suppressing those structures. Note that some modification strategies allowed considerable advances in improving general characteristics of lithium–metal batteries [13, 14], but the problem is on the whole far from solution. It becomes particularly important to understand how the SEI is formed on a metal anode. Controllable formation of the stable and most homogeneous possible SEI layer that prevents a reaction between the anode lithium and the electrolyte but does not block the cation transport may enable the use of metallic lithium as an anode.

2.2.3. Lithium–oxygen batteries. Record high theoretical specific capacities ($>700 \text{ mA h/g}$) characterize batteries of the lithium–oxygen type with carbon cathodes and lithium anodes. Interaction of lithium with oxygen in electrochemical cells occurs at the inner surface of the nanopores of the carbon material impregnated with the liquid electrolyte. Lithium is electrodeposited in them in the form of inhomogeneous structures insoluble in the electrolyte (lithium peroxide Li_2O_2). The discharge capacity can be limited due to both passivation of the electrode by nonconductive products and obstructed diffusion of active components in the electrolyte because of blocked pores. It is practically reflected by that the discharge voltage profile is terminated long before the theoretically possible capacity limit. To minimize this sort of spurious processes is a currently important objective,

fulfilment of which may raise development and applications of electrochemical energy storage device to a completely different level.

3. STRUCTURAL INVESTIGATIONS USING NEUTRON SCATTERING METHODS

Structural investigations of electrochemical systems are carried out using mainly elastic neutron scattering methods, including Bragg diffraction, reflectometry, and small-angle scattering. In situ experiments are usually conducted on flat assemblies in special electrochemical cells with current and voltage control during discharge/charge. Each method applies to different structural features. In structural diffraction experiments, scattering from ordered atoms of assembly components is detected. In reflectometry, beam deflections at surfaces of model planar electrodes with a layered structure and low roughness of interfaces are analyzed. In the case of small-angle scattering, beam broadening takes place due to scattering from inhomogeneities in assembly components.

Owing to the fact that the materials mainly used in common LIBs have the crystal structure, and an experimental geometry is much simpler as compared to other methods, the largest number of publications in topical journals deal with Bragg diffraction studies of the atomic structure of LIB electrodes.

The currently increasing interest in the reflectometry and small-angle scattering methods for investigation of lithium batteries is determined by two factors. First, important processes occur in the immediate vicinity of the electrochemical interface to which the reflectometry and small-angle scattering methods are sensitive, unlike structural diffraction. Second, prospects of lithium batteries are more and more associated with nanostructured materials that are naturally suitable systems for studies by the reflectometry and small-angle scattering methods.

3.1. Bragg Diffraction

Diffraction is now a standard method for defining structural characteristics of a crystalline material. Most electrodes in lithium-ion batteries are based on polycrystalline materials that are studied using neutron diffraction. Wavelengths of thermal neutrons (energy $1\text{--}300 \text{ meV}$) range from 0.05 to 1 nm . In a neutron diffraction experiment, the main contribution to the scattering most often comes from elastic nuclear scattering—scattering from nuclei (additional magnetic scattering becomes substantial in the case of ordering of magnetic atoms). Analysis in terms of possible radiation energy variation is not performed in such experiments.

Diffraction on crystals is described within the inverse grating formalism: diffraction peaks are observed when the Wulff–Bragg's condition is fulfilled, i.e., the scattering vector q and the inverse grat-

ing vector coincide in magnitude. Positions of peaks in the diffraction pattern are determined by the symmetry and size of the elementary lattice cell. Intensity of diffraction peaks depends on the structural factor whose value is determined by the positions and type of atoms and the population of atomic positions in the elementary cell. The general problem that can be solved using neutron diffraction on a crystal is reconstruction of the distribution of the scattering nuclear or magnetic density in the elementary cell. To this end, diffraction peak intensities should be measured, absolute values of structural factors determined from them, their phases found in whatever way, and the inverse Fourier transform should be performed for coherent scattering lengths $b(r)$ or magnetic density $m(r)$. If the model of the structure is known, its characteristics (elementary cell parameters, coordinates of atoms, their thermal factors, position filling factors, magnetic moment, etc.) can be specified by minimizing the functional constructed from the differences of the measured and calculated intensities.

For diffraction on a crystal to occur, coherent neutron scattering is required (constant wave phase difference in the scattering). Stochastic disturbances in atomic ordering (long-range disordering) give rise to incoherent background scattering (random wave phase difference variation in the scattering). These disturbances include lattice distortions and defects, random distributions in occupation of atomic positions, and atomic thermal vibrations. Spatial correlations can partially occur in these processes resulting in background scattering in the vicinity of the diffraction peaks, which is diffuse scattering that carries information on local disorder in the crystal structure. It is analyzed using the pair distance function (PDF) (an analog of the radial distribution function in scattering by liquids) that allows judging whether there is the short-range order. Thus, it may be said that in a real crystal, apart from the long-range order that yields diffraction peaks— q modulation of coherent scattering, there are crystal lattice disordering and other short-range order imperfections that produce diffuse scattering— q modulation of incoherent scattering.

In neutron scattering, there are additional contributions to the incoherent scattering that are related to the specific feature of the radiation. Since thermal neutrons have low energy, collective thermal motion of atoms leads to inelastic neutron—phonon scattering that contributes to diffuse scattering. There is also isotopic incoherence caused by the presence of a few isotopes, each with its own scattering length, in the natural mixture of crystal substance nuclei. Finally, spin incoherence arises from the difference in scattering lengths of neutrons with different mutual spin orientation of the neutron ($\pm 1/2$) and the scattering nucleus. This is best manifested in hydrogen; therefore, isotopic substitution of deuterium for hydrogen is often used to suppress this contribution. Contributions from isotopic and spin incoherence do not depend on q and

constitute a background in diffraction patterns. Incoherent scattering naturally “takes away” useful intensity from coherent scattering, which increases the background.

The width of the diffraction peaks is determined by the resolution of the diffractometer, the size of the crystal’s coherent scattering region (atomically ordered region that coherently scatters radiation independently of other similar regions and is often close in size to a crystallite or a grain), and possible crystal structure microdeformations (elementary cell size fluctuations caused by displacement of atoms from their ideal position that may occur, for example, due to packing defects or presence of dislocations in the crystal).

Thus, the diffraction experiment yields information on the phase composition, crystal structure and its local distortions resulting from different causes, and microstructure of the crystalline substance. Indirectly, from the data on positions of atoms in an elementary cell and calculations of valence distances, it is possible to get information on more specific characteristics of crystalline materials for LIBs, e.g., diffusion paths of lithium ions. In X-ray diffraction (XRD) experiments, hydrogen and lithium are hardly visible because of a small form factor for light atoms. In neutron diffraction experiments, there is no such problem: the coherent scattering length, which is an analog of the atomic factor for neutrons, irregularly varies with respect to the atomic mass. However, in the neutron diffraction experiment one often uses electrolytes based on deuterated solvents to decrease the incoherent hydrogen background, which substantially increases the cost of the experiment. An important factor is very weak (compared to X rays) absorption of neutrons in the medium. Only few elements and isotopes strongly absorb thermal neutrons. Consequently, neutrons can penetrate rather deep (few centimeters) into substance, which makes it possible to study bulk materials and rather large engineering products like batteries and accumulators.

Electrochemical characteristics of materials for batteries are determined not only by their elemental composition but also by the organization of the crystalline structure and microstructure and by the phase composition. Diffraction methods, including neutron diffraction, play one of the crucial roles in establishing a relation between the structure and the properties of these materials. Some examples of applying neutron diffraction to characterization of modern materials for lithium batteries in some neutron centers can be found in the recent review [6].

At FLNP, the standard neutron diffraction method was used from 2013 to study powders of electrode materials and solid electrolytes at the IBR-2 reactor with the diffractometers HRFD [15] and RTD [16]. In [17], LiFePO_4 powders in the initial state (LFP) and doped with vanadium (LFPV) were investigated. High-resolution neutron diffraction helped explain

why LFPV has better electrochemical properties (~15% higher capacity) than LFP: analysis of variations in the microstructure of the cathode material when vanadium was added to it showed a considerable increase in the degree of structure imperfection corresponding to a decrease in the coherent regions of the cathode material (effective crystallite sizes) and an increase in the effective area of their contact with the electrolyte, which allowed deeper charge/discharge of the cathode particles during the investigations.

Effective high-resolution neutron diffraction investigations of $\text{LiNi}_{0.5}\text{Mn}_{1.5}\text{O}$ powders doped with Co, Cr, Ti, Al, and Mg cations were carried out together with the Institute of Solid State Chemistry and Mechanochemistry (Novosibirsk, Russia). It is known that depending on its synthesis conditions, spinel $\text{LiNi}_{0.5}\text{Mn}_{1.5}\text{O}_4$ can crystallize into two alternative structures with identically sized elementary cells: a cation-ordered face-centered cubic structure with the $Fd-3m$ space group or an ordered structure with the $P4_332$ primitive cell. The highest capacity is predominantly characteristic of the compositions described by the disordered structure. To differentiate between these two types of structure using X-ray diffraction is hardly possible because the atomic form factors of Mn and Ni are close in value. At the same time, the neutron scattering lengths are so different that the given phases are easily identified and discriminated from each other in the neutron diffraction experiment. Neutron diffraction allows us to determine how temperature and the type of doping cation affect formation of various cubic phases and which of the basic cations (Ni or Mn) is displaced by the doping cation. Experiments showed that dopants mainly displaced nickel cations [18]. The samples synthesized at high temperatures are almost free of the ordered $P4_332$ phase (2–6%). In the samples synthesized at lower temperatures the amount of the ordered phase is much larger, approaching 10%. The best electrochemical characteristics were shown by the samples doped with Cr and Ti and synthesized at high temperatures.

High-resolution neutron diffraction was also used at FLNP to investigate materials holding promise as solid electrolytes for LIBs. Rechargeable batteries with solid electrolytes have advantages over traditional batteries with liquid electrolytes: higher voltage, extended working temperature range, longer service life, environmental friendliness, and safety due to minimized electrolyte fire and leakage risk. In 2016, the crystal structure and lithium migration paths in Li_2ZrO_3 and $\text{Li}_{1.8}\text{ZrO}_{3-\delta}$ were investigated at high temperatures (from room temperature to 833 K, a total of seven temperature points) [19]. Lithium zirconates were considered as promising lithium-conducting materials for coating cathode particles to prevent their degradation when in contact with various aggressive components. The experiments (Fig. 3) resulted in obtaining the temperature evolution of parameters of the mono-

clinic structure (space group $C2/c$), including populations of both lithium positions. It was found that both compositions were lithium deficient at room temperature and exhibited an ion conduction jump at about 740 and 710 K respectively. It was shown that depopulation of fully occupied Li positions under heating correlated well with the conduction behavior and favored diffusion of Li^+ ions through the bottleneck in the lithium zirconate structure.

As was already mentioned above, the crystalline structure of the electrode materials is closely related to the characteristics of lithium-ion energy storage devices, including power, energy density, capacity, cycling, etc. The most difficult in terms of implementation and data analysis are investigations conducted during the operation of the electrochemical cell/battery. However, the value of the gained information can hardly be overestimated, since in this case the state of the battery material structure is monitored directly during battery operation, showing all possible phases, structural transformations, and other structure features inaccessible in investigations outside the functioning object (e.g., investigation of unstable intermediate phases of an electrode material relaxing to some stable state). For these purposes, electrochemical cells specially designed for a particular diffraction experiment geometry and called model cells are most often used.

In the past decade, structural in situ/operando neutron diffraction has been actively used to track structure evolution of various electrodes (see [1, 6, 20]). Here, we highlight the main current capabilities of this method with application to lithium energy storage devices using as an example implementation of in situ and operando electrochemical diffraction investigations at the IBR-2.

From the point of view of electrochemical characteristics as applied to the investigation of cycling processes, diffraction cells for model studies should be copies of standard laboratory electrochemical cells in which new materials are tested. While developing (see [6, 20]), initially cylindrical cells (based on cylindrical containers of materials weakly absorbing neutrons) changed to more complicated but more efficient designs for the purposes of studying the electrochemical component. Specifically, in the research cells where the counter electrode is a material other than lithium, a three-electrode system is desirable for voltage/current control. While functioning, the working electrode suffers changes that influence the potential difference between the working electrode and the counter electrode. This influence is compensated and adjusted by the external potentiostat. To independently control the potential, a third, reference, electrode is included in the scheme, which allows processes in the anode and cathode materials to be investigated separately. Also, both the full and the halved configurations is used. In the latter case, the standard

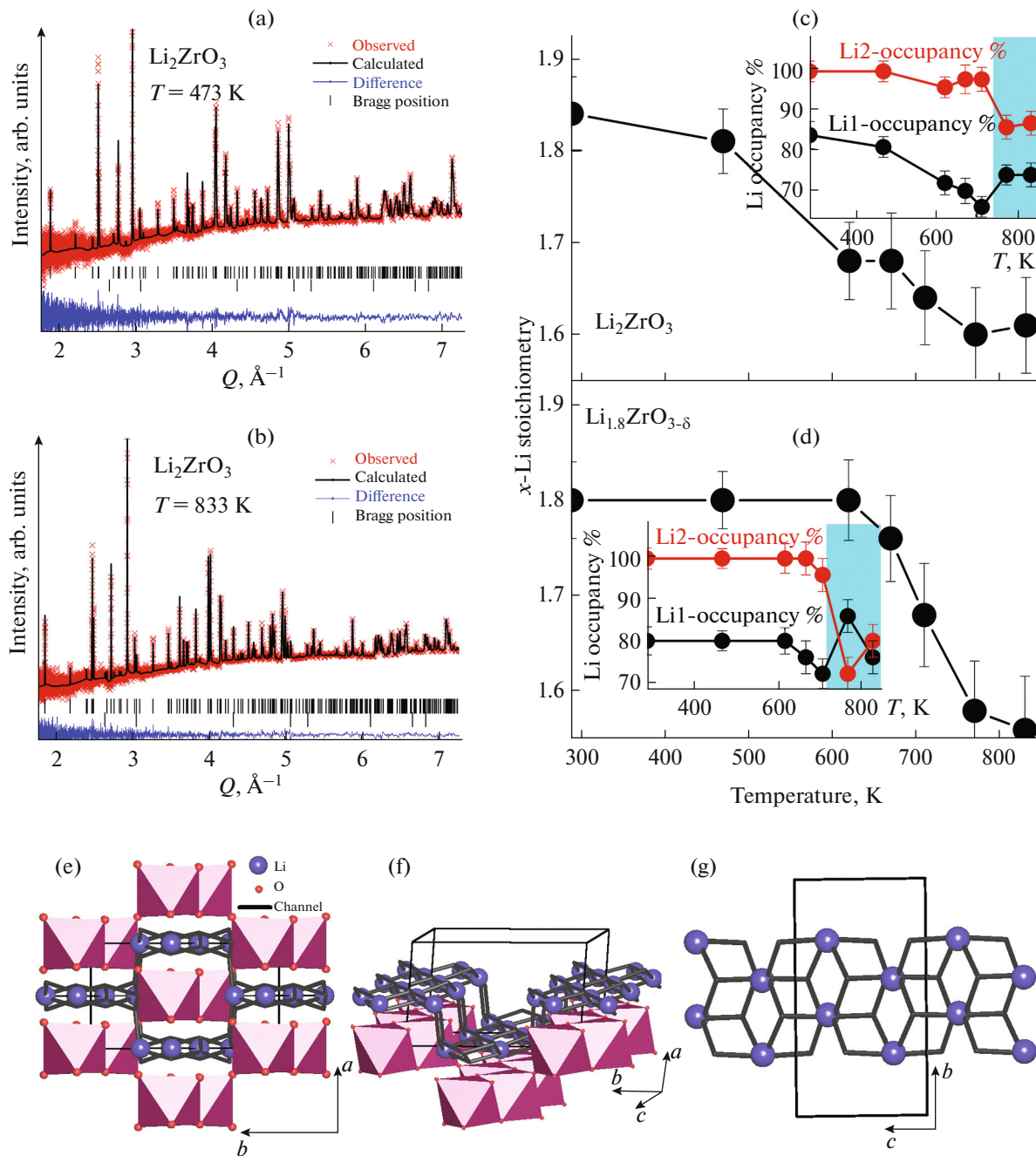


Fig. 3. Neutron powder diffraction patterns of Li_2ZrO_3 (a, b) measured by the HRFD diffractometer JINR IBR-2 at 473 and 833 K and analyzed using the Rietveld method. Symbols are experimental intensities; solid black lines show the results of the fit. Difference between the calculated and observed intensities is shown at the bottom. A row of vertical marks under the plot refers to nuclear Bragg peaks. Temperature dependence of the Li^+ ion stoichiometry and the occupancy of octahedral interstitial lithium atoms for Li_2ZrO_3 (c) and $\text{Li}_{1.8}\text{ZrO}_{3-\delta}$ (d). Crystal structure and migration paths (e, f, g) for the Li_2ZrO_3 and $\text{Li}_{1.8}\text{ZrO}_{3-\delta}$ samples constructed on the basis of the experimental neutron diffraction data. Red and blue show oxygen and lithium atoms respectively. Black lines show migration channels of lithium ions. Colored pink are ZrO_6 octahedra. The figure is reproduced by permission from [19] (©Elsevier, 2021).

electrode, being also the reference electrode (usually lithium, as already mentioned), is used as the counter electrode.

Current coin-type cells are flat assemblies tightly sealed by the clamping flanges, either round or rectangular in shape. In coffee bag cells, smaller-sized

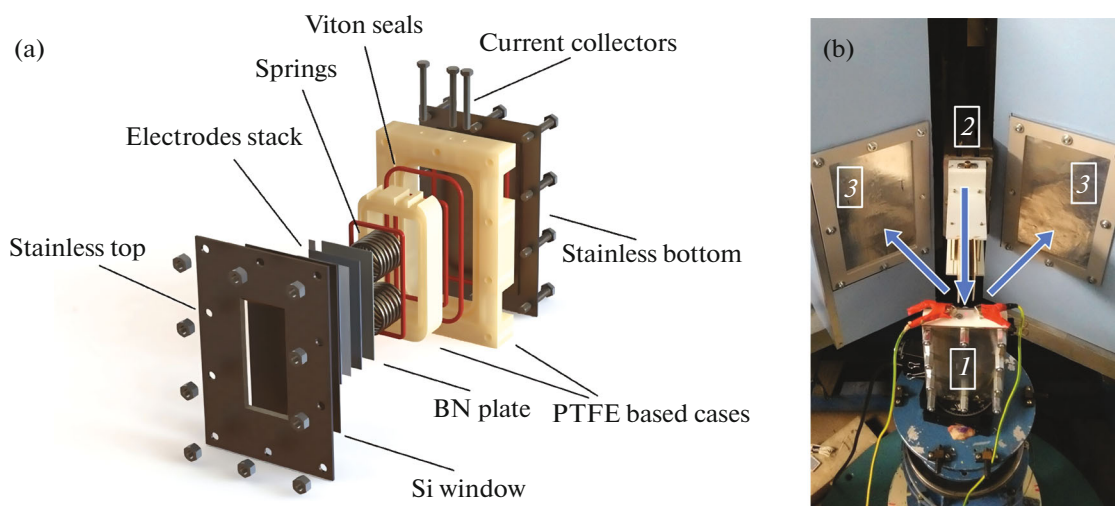


Fig. 4. Schematic view of the NPD electrochemical cell (a) and photo of its installation at the HRFD time-of-flight diffractometer at the JINR IBR-2 pulsed reactor (Dubna, Russia) (b); (1) cell, (2) beam aperture, (3) backscattering detectors; arrows indicate directions of the neutron beam and the scattered neutrons. The figure is reproduced by permission from [21] (©Elsevier, 2021).

assemblies are placed in a bag of a weakly absorbing material (aluminum for neutrons) subsequently filled with a liquid electrolyte and tightly sealed. In Swagelok cells, the assembly is placed in a larger container of standard metallic pipes with tight sealing ensured by the side flanges. Unlike the case in other types of cells, standard flanges allow a wide diversity of configurations with metal current collectors. In particular, this concerns the three-electrode configuration of the experiment. This type of cell also ensures fast polarity reversal. In diffraction cells, both the reflection configuration and the transmission configuration are used. The *transmission* geometry allows complete penetration in all assembly elements (electrodes, electrolyte, separator, current collector). It is important that the entire depth of the working electrode is involved, rather than only its surface layer whose thickness depends on the angle of incidence of the beam and the composition of the material. In the case of transmission cells, structural information can simultaneously be obtained from the anode and cathode materials. However, if structural changes are inhomogeneous, it is impossible to determine inhomogeneity distribution over the volume of the electrode (e.g., to find out whether they occur near the current collector or near the separator). At the same time, the *reflection* configuration allows a higher resolution because large scattering angles are used. In coin-type and Swagelok cells, housings of the structure for beam passage should have windows of a weakly absorbing material (aluminum, quartz, and sapphire for neutrons). This gives rise to a number of potential problems in the operation of these cells: electrolyte leakage is possible, cell housings with windows can cause nonuniform pressure, and windows where insulation materials are used can impair the electric connection with the elec-

trode. It is known that thick cathodes cause inhomogeneous electrochemical reactions. As an example of recent developments, Fig. 4 shows the diffraction cell (coin type) for the neutron diffraction experiment and photos of its installation at the diffractometer. Note that the presented neutron diffraction cell is characterized by a rather high degree of cyclability (over 500 charge/discharge cycles without significant efficiency decrease at the current of ~ 10 mA).

To collect sufficient statistics for analysis in neutron diffraction experiments, cell charge/discharge is usually performed at a low rate. The discharge/charge rate is designated as nC , where C is the material capacity, and n is the fraction of an hour in which discharge/charge is performed. The value $n < 1$ means that the discharge/charge time is increased to $1/n$ hours; in this case, the designation C/k is often used, where $k = 1/n$ is an integer. At small n (high charge/discharge rates) and with the same time exposure of diffraction pattern accumulation, a substantially larger set of observable diffraction data can be obtained from the materials of the electrochemical cell under investigation. In [17], in situ neutron diffraction was used to study processes during charge-discharge of lithium batteries with a standard cathode based on LFP and on LFPV (1 wt % vanadium doping) and an anode based on graphite (Fig. 5a). Diffraction measurements were performed at different states of charge (SOC). Neutrons make it possible to thoroughly track (Figs. 5b, 5c) the multistage process of Li insertion in graphite with subsequent formation of several phases LiC_n and the process of reversible conversion of LiFePO_4 to FePO_4 . As compared to LFP, a large part of the anode material converts to the final LiC_6 state. Also, in LFPV, as compared to LFP, crystallites noticeably decrease in size, which correlates with the best electro-

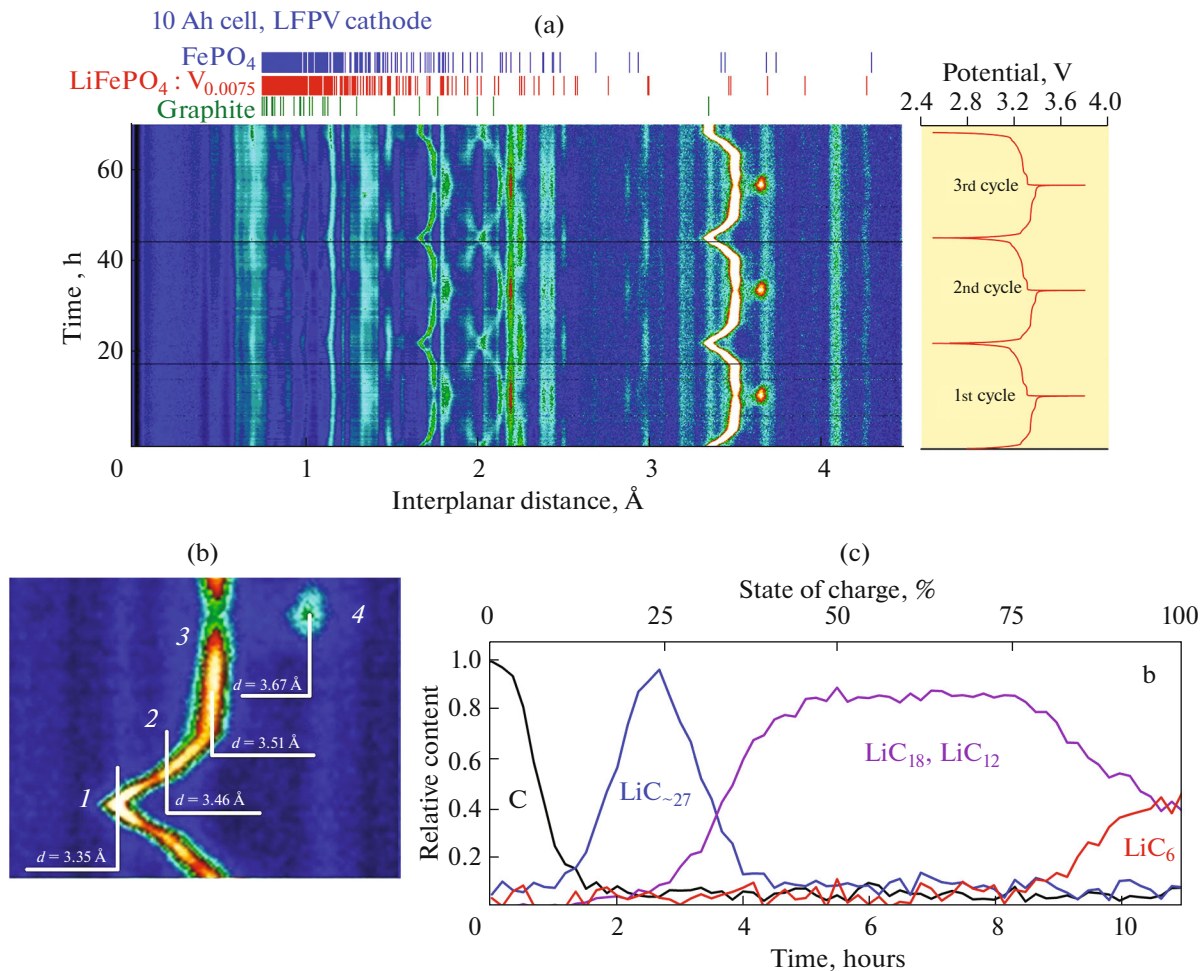


Fig. 5. (a) In situ/operando NPD diagram for the cell with the cathode based on the vanadium-doped LFP (LFPV) and the graphite anode for three full charge/discharge cycles (rate 0.1C). Vertical line bars at the top indicate positions of diffraction peaks for the electrode components of the cell in their initial state. (b) Diffraction peak evolution showing phase change in the anode. (c) Content of different LiC_n phases in the anode during one charge cycle as a function of time (lower scale) and SOC (upper scale) found from relative variations in intensities of the corresponding diffraction peaks. The data are obtained using the HRFD time-of-flight diffractometer at the JINR IBR-2 pulsed reactor (Dubna, Russia). The figure is reproduced by permission from [17] (©Elsevier, 2021).

chemical properties of this material. This sort of information is used to study how modification of electrode materials (e.g., doping) affects evolution of the electrode structure. Another interesting problem is reproducibility of structural evolution of electrode materials. This allows judging how they structurally degrade in the process of functioning.

High resolution in neutron in situ diffractometry allows efficient study of phase separation in electrodes. For example, in the NCA cathode, $\text{Li}_x\text{Ni}_{0.8}\text{Co}_{0.15}\text{Al}_{0.05}\text{O}_2$, two-phase separation was observed during the first charge (Fig. 6) [21]. The effect arises from compaction of electrodes during synthesis, which leads to formation of nucleus–shell structures of crystal grains in cathode materials. It was found out that stronger compaction of electrodes partially suppresses phase separation of the cathode material: the SOC range in which two

phases coexist decreases, as also does the difference between structural parameters of phases.

3.2. Reflectometry

Neutron reflectometry (NR) detects reflection of a plane-collimated beam from a flat interface. The penetrating nature of the radiation allows efficient study of the hidden interface between the surface of a thin (<100 nm) electrode on a substrate and a liquid electrolyte (see the pictorial diagram of the experiment in Fig. 7). A special electrochemical cell is used to direct the beam to the interface through a moderately absorbing solid substrate (crystalline silicon, quartz). The incident and reflected beams go into/from the experimental cell through the side “windows” at a large grazing angle, i.e., without significant reflection. The circuit is constructed using special connectors to

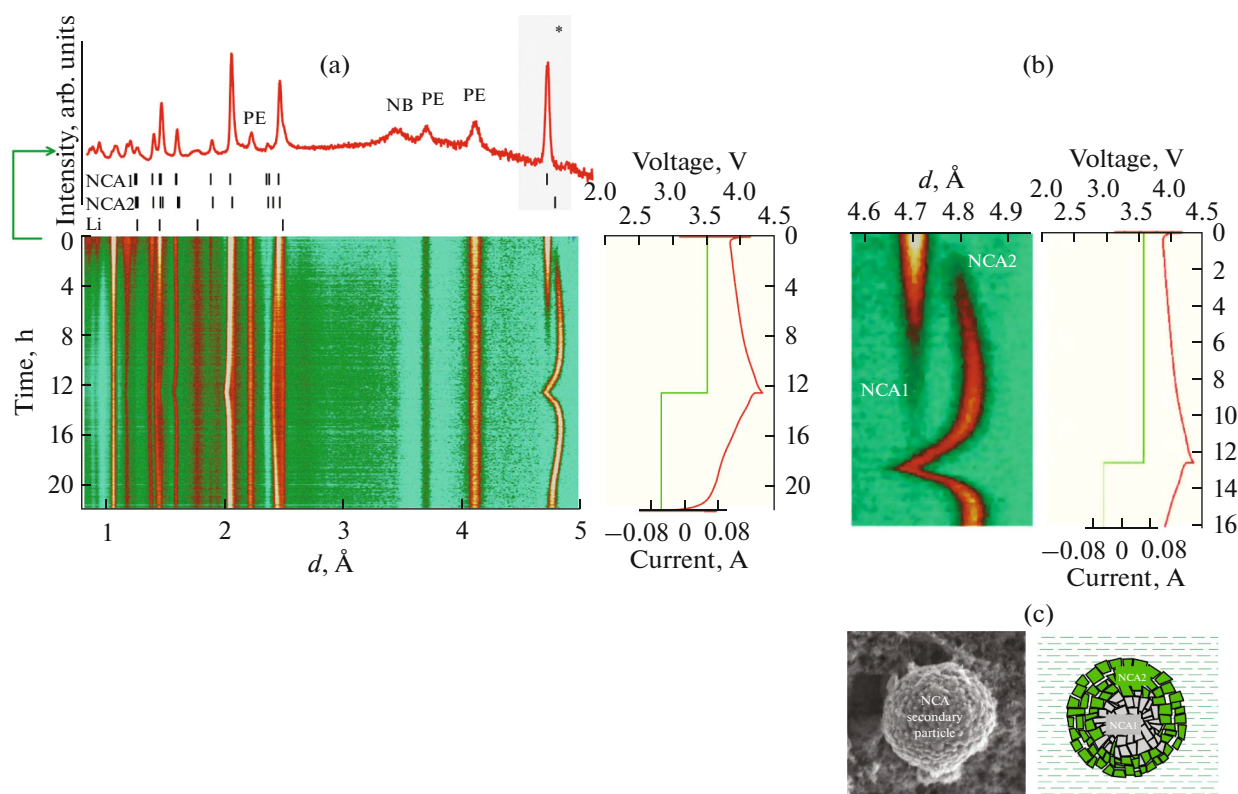


Fig. 6. (a) In situ/operando NPD diagram for the cell with the NCA-based cathode at the first charge/discharge cycle (rate 0.1C). The cathode material is structurally divided into two crystal phases, NCA1 and NCA2. Calculated positions of the diffraction peaks of NCA1, NCA2, and Li are shown by vertical line bars. Also shown are diffraction peaks of other materials: boron nitride (NB), the polyethylene separator (PE), and the lithium anode. The NCA 003 diffraction peak is marked with an asterisk. (b) Zoomed region with the evolution of the diffraction peak in the vicinity of the NCA 003 peak. (c) Model of the two-phase structure of NCA granules with the complementary SEM data. The data are obtained using the HRFD time-of-flight diffractometer at the JINR IBR-2 pulsed reactor (Dubna, Russia). The figure is reproduced by permission from [21] (©Elsevier, 2021).

connect the working and counter electrodes to the potentiostat for adjusting the potential and the current in the circuit. At rather small grazing angles (on the order of milliradians) there is total or partial reflection from interface depending on the scattering vector component normal to the interface q_z . Decay of the coefficient of specular reflection R (fraction of beam intensity reflected from the interface) in the region of partial reflection (large q_z) is modulated through the Fourier transform by the scattering length density distribution (SLD) (atomic form factor) along the normal to the interface. The dependence $R(q_z)$ is sensitive to formation of nanostructures (effective thickness 1–100 nm) at the interfaces and enables simulation of the SLD with lateral averaging (along the interface). In the specular reflection analysis, the SLD is simulated as a set of layers, each having a certain thickness and SLD, and each transition between layers is approximated by the Gaussian profile with the width related to the average roughness of the interlayer boundary. This approach implies that the roughness parameter is small. Roughness leads to scattering in the nonspecular channel (direction x), which known as diffuse, or

nonspecular, scattering. Scattering in the specular channel correspondingly decreases. Diffuse scattering is also present in the specular channel. Because of the finite width of the incident beam, in the reflected beam there are waves with different directions distributed around the specular direction of the beam. These directions broaden due to diffuse scattering and overlap with the specular direction. Low roughness allows relatively simple correction of the specular channel data by subtracting the diffuse scattering background in the vicinity of the specular reflection peak. The NR resolution in experiments with current neutron sources is on the order of or slightly lower than 1 nm.

Experience in experimental studies of planar electrochemical interfaces with liquid electrolytes under different conditions (including oxidation of the surface, electrolytic deposition, ion distribution in liquid carriers in subsurface layers near electrodes) and other electrochemical problems of specular neutron reflectometry are reviewed at length in [2].

The NR electrochemical cell for in situ experiments is based on a possibility of using a massive single-crystal substrate (silicon or quartz) round or rect-

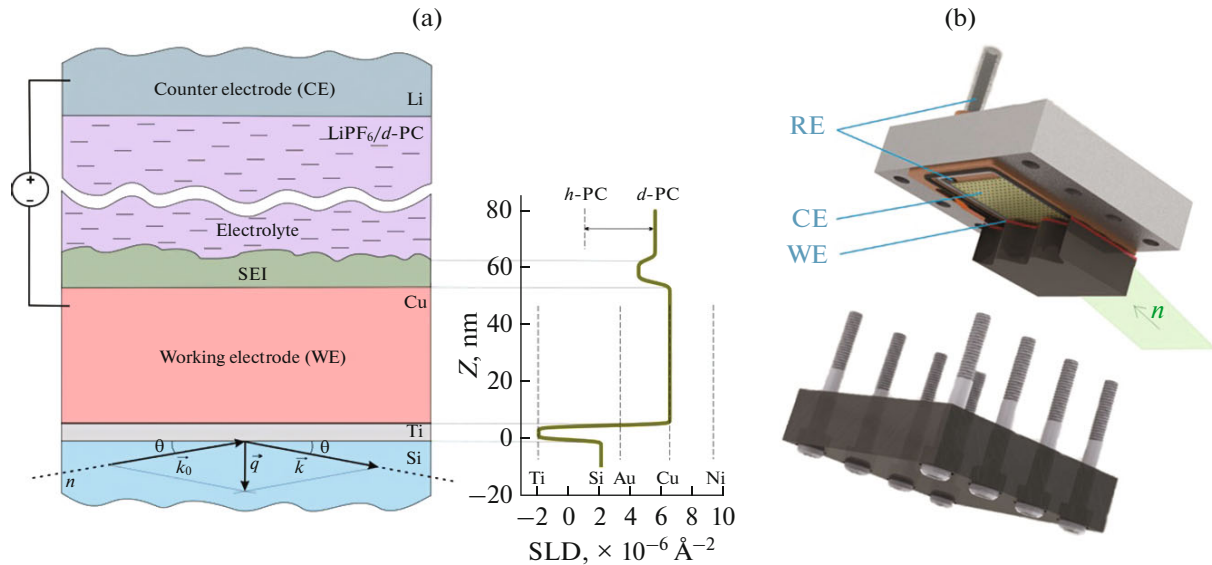


Fig. 7. (a) Pictorial diagram of the specular NR experiment at the electrochemical interface of the metal electrode and the liquid lithium-containing electrolyte. SLD profiles of the interface are schematically shown with possible spectrum of electrode materials and combinations of h-/d-electrolytes. (b) Design of the electrochemical cell for NR experiments with liquid electrolytes. WE is the working electrode, CE is the counter electrode, and RE is the reference electrode. The figure is reproduced by permission from [27] (©Elsevier, 2019).

angular in cross section with the optical path of up to 8 cm and thickness of up to 1.5 cm onto which a thin-film electrode (working electrode) with a different layered structure depending on the objective is deposited by sputtering (mainly magnetron sputtering). Sometimes, the substrate itself is a working electrode, and deposition of additional layers is not needed. The thermal neutron transmittance of the substrate is $\sim 80\%$. Development of the design and implementation principles can be found in [22–30]. This problem is generalized in the recent review of NR applications [31]. The pictorial diagram of a modern electrochemical cell of this kind is shown in Fig. 7b. One of the first successful applications of reflectometry at the NIST neutron reactor (United States) was detection and study of formation and evolution of the SEI layer on a copper electrode [32] in the process of cycling. In the widely used scheme of cell arrangement at reflectometers with the horizontal sample geometry, the substrate is above the liquid component. However, there are cases where the electrolyte is above the substrate, which allows the filling of the cells with a liquid electrolyte to be more efficiently controlled and consumption of rather expensive deuterated components to be decreased. At present, NR measurements using electrochemical cells can be carried out in almost all neutron centers with a high-intensity neutron source.

At FLNP, neutron reflectometry experiments on electrochemical interfaces like that in Fig. 7 have been conducted since 2017 [27] at the GRAINS reflectometer [33]. To determine the depth distribution of the SLD in the NR experiment of this type is fairly simple

from the point of view of interpreting the reflection curve. There is a preset initial configuration of the interface region. Deposition of the electrode is highly accurately controlled from the air using laboratory instruments in a standard XRR experiment. After that, the SLD profile is checked in the NR experiment, first without and then with electrolyte filling. Thus, before the interfaces change during electrochemical processes, there is detailed information on the initial configuration. In the course of in situ and operando investigations, parameters of the initial configuration are fixed, and it is necessary to determine a rather limited number of parameters of a new layer (layers), including thickness, roughness, and average SLD of each layer. The difficulty is that interface variations at the initial stages of discharge/charge are rather small from the point of view of reflectometry, and the limited range of the scattering vector simultaneously detected within one exposure limits the resolution. In this connection, it is matter of principle for NR to use the time-of-flight mode, where the scattering (reflection) is fixed, and scanning is along the wavelength. It is a standard mode for pulsed sources, while for stationary neutron sources a mechanical slit chopper is installed in the beam to ensure the pulsed mode. Considerable loss of the average beam intensity makes this mode possible only at high-intensity stationary neutron sources.

Optimization of the initial configuration for increasing sensitivity of NR experiments to small variations at interfaces during the functioning of the cell was discussed in [27, 34, 35]. The goal is to select con-

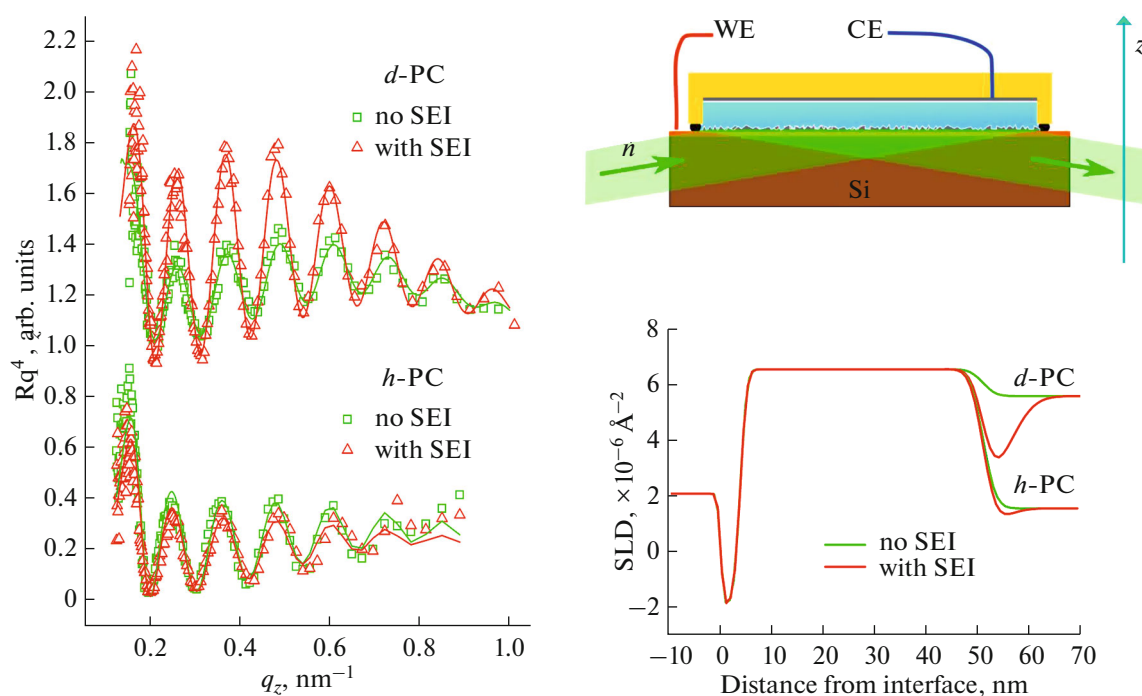


Fig. 8. Contrast variation in the NR experiment on formation of the SEI on the copper electrode (single-crystal silicon substrate) in contact with the liquid electrolyte of 0.1 mol/L LiClO_4 in PC. SEI formation regime: +10 mV relative to the reference electrode, 15 min. Variations in the reflection curves (Fresnel representation) and the corresponding SLD profiles in the case of the fully deuterated (d-PC) and fully protonated (h-PC) liquid base are shown. Formation of the SEI is manifested as an additional peculiarity between Cu layer and the electrolyte, which is better seen in the case of h-PC. Apart from the Cu layer (nominal thickness 50 nm), a thin Ti layer (nominal thickness 5 nm) additionally deposited to improve Cu adhesion is seen in the profile. The experimental data are obtained using the GRAINS time-of-flight reflectometer at the JINR IBR-2 pulsed reactor (Dubna, Russia). The figure is reproduced by permission from [36] (©Elsevier, 2019).

trast between the components so that appearance of a new thin layer at an interface causes strong changes in reflectometry curves. General optimization is a rather complicated problem, but there are practical limits on variation of interface parameters, which appreciably narrows the phase space regions where optimization should be performed. Most preferable are the cases where the electrolyte SLD coincides either with the substrate SLD (e.g., [32]) or with the electrode SLD (e.g., [27]). Figure 8 demonstrates NR sensitivity to formation of the SEI on the copper cathode in the case of a fully deuterated and a fully protonated electrolyte. Thus, there is currently a wide range of NR approaches to conduct in situ and operando experiments with ensuring contrast variation and maintaining the same conditions for electrochemical processes at interfaces.

Neutron reflectometry is involved in active studies of metal anode systems for nonintercalation lithium-ion batteries. As pointed out above, determination of parameters of the SEI on the anode surface is an important applied problem. Formation of the SEI is itself an open question that requires general investigation. It is also important that the SEI can be associated with occurrence of needle-shaped formations at the anode surface. Lithium, the most promising anode

material from the viewpoint of capacity characteristics, is a very difficult material to be used for controllable production of thin-film electrodes on substrates; therefore, other model metals are used. First of all, to increase the quality of the experiment, materials without lithium intercalation are taken [32]. In this case, the reflection curve variations are strictly caused only by the new layer at the electrode surface. During the experiment, reflection curves are obtained at different points of the current–voltage diagram, including cycling. Evolution of the SLD profile obtained from the reflection curves shows continuous SEI structure variation in the course of the discharge/charge cycle. The thickness and scattering length density of the layer are analyzed with respect to its possible composition and variation during charge/discharge cycles.

In the NR experiments at the IBR-2 reactor carried out in collaboration with the Faculty of Chemistry of Moscow State University (MSU), Dubna State University, and Kyiv National University, deposition on the metal electrode after the formation of the SEI layer was studied [27, 36] (Fig. 9). A special cell was developed for the experiments [37]. Lithium intercalation was eliminated by using a copper electrode; only the layer deposited on the metal surface was allowed. The effect of the nonelectroactive additive (0.5 mol/L

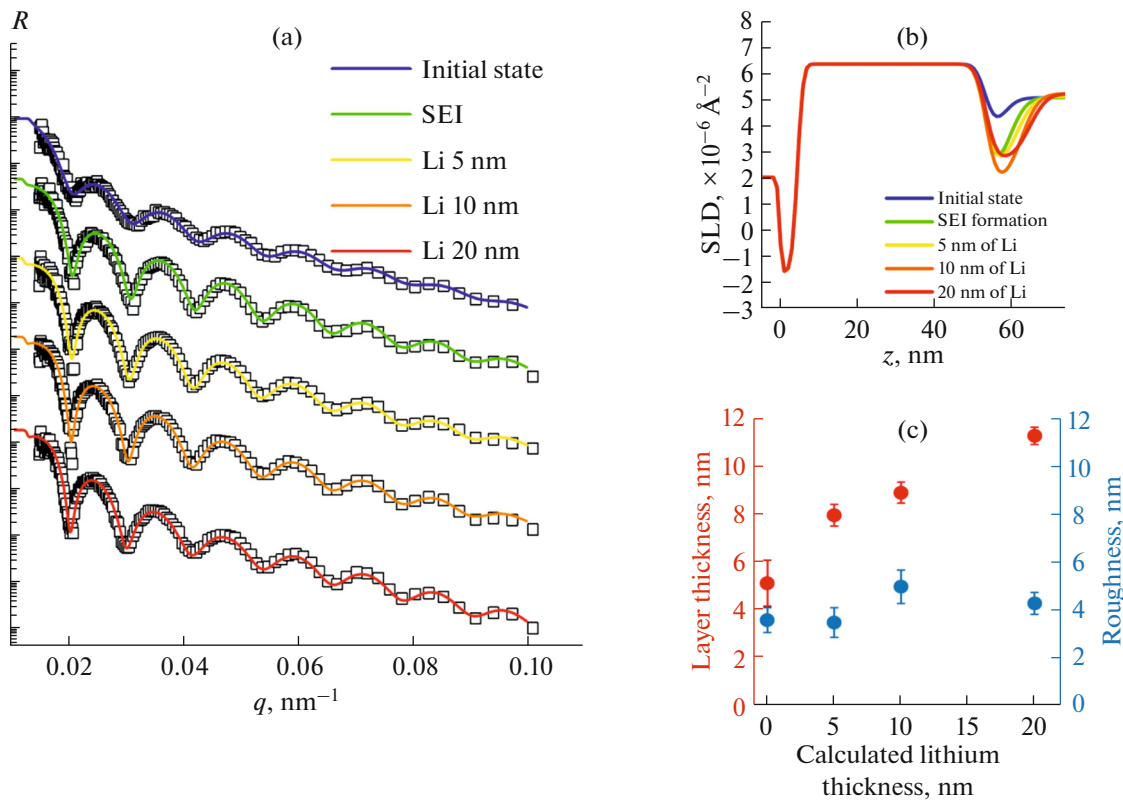


Fig. 9. (a) Experimental results (data points) of specular neutron reflection and results of the approximation (solid curves) for the deposition of lithium on the planar copper electrode from the liquid electrolyte after the formation of the SEI layer. The inscriptions at the curves indicate the nominal thickness of the deposited lithium calculated from the known electric charge passed through the cell on the assumption of the homogeneous Li layer density. The data are separated along the coordinate axis for convenience. (b) SLD profiles corresponding to the model reflection curves. (c) Dependences of the average thickness and roughness of the deposited layer (SEI + Li) on the nominal thickness of the Li layer. The experimental data are obtained using the GRAINS time-of-flight reflectometer at the JINR IBR-2 pulsed reactor (Dubna, Russia). The figure is reproduced by permission from [27] (©Elsevier, 2017).

TBAP) in the electrolyte (0.1 mol/L LiClO₄ d-PC) supposed to suppress growth of dendrite formations was considered. This modification of the electrolyte causes considerable changes in the character of lithium deposition according to the NR data (Fig. 10). From the point of view of the SLD distribution, a core layer enriched in lithium and a transition layer presumably caused by needle-shaped structures can be distinguished. Inhomogeneous structures are responsible for the access of the solvent to the external layer and the difference between the nominal thickness of the uniformly deposited lithium layer (calculated from the known passed charge) and the observed thickness. The transition layer is poorly resolved in NR experiments while characteristic features of the core layer can be compared for different electrolyte compositions. It is shown that TBAP suppresses the core layer and appreciably changes its composition.

Experiments of this kind focused on determination of the composition and evolution of the SEI layer on the tungsten electrode are described in [28, 30], where a conclusion is drawn about the two-level organization

already at the SEI level. The internal dense SEI layer (thickness up to 3.7 nm) consists mainly of lithium oxide Li₂O, while the external layer (thickness up to 15.4 nm) is much more inhomogeneous (porous) and consists of organic compounds.

3.3. Small-Angle Scattering

The small-angle neutron scattering method detects broadening of the initially rather narrow axial beam moving through a system with inhomogeneities having a characteristic size on the order of 1–100 nm. The broadening angle is smaller than 10° (which gave the name to the method); scattering vectors of the detected radiation almost entirely lie in the plane normal to the beam. Detection is by a large-area position-sensitive detector placed behind the sample. The differential cross section of the small-angle scattering is measured by unit volume (traditionally, but somewhat improperly called the scattering intensity). If there is no texture, averaging over all scattering vector orientations effectively occurs in the sample. In this case, 2D

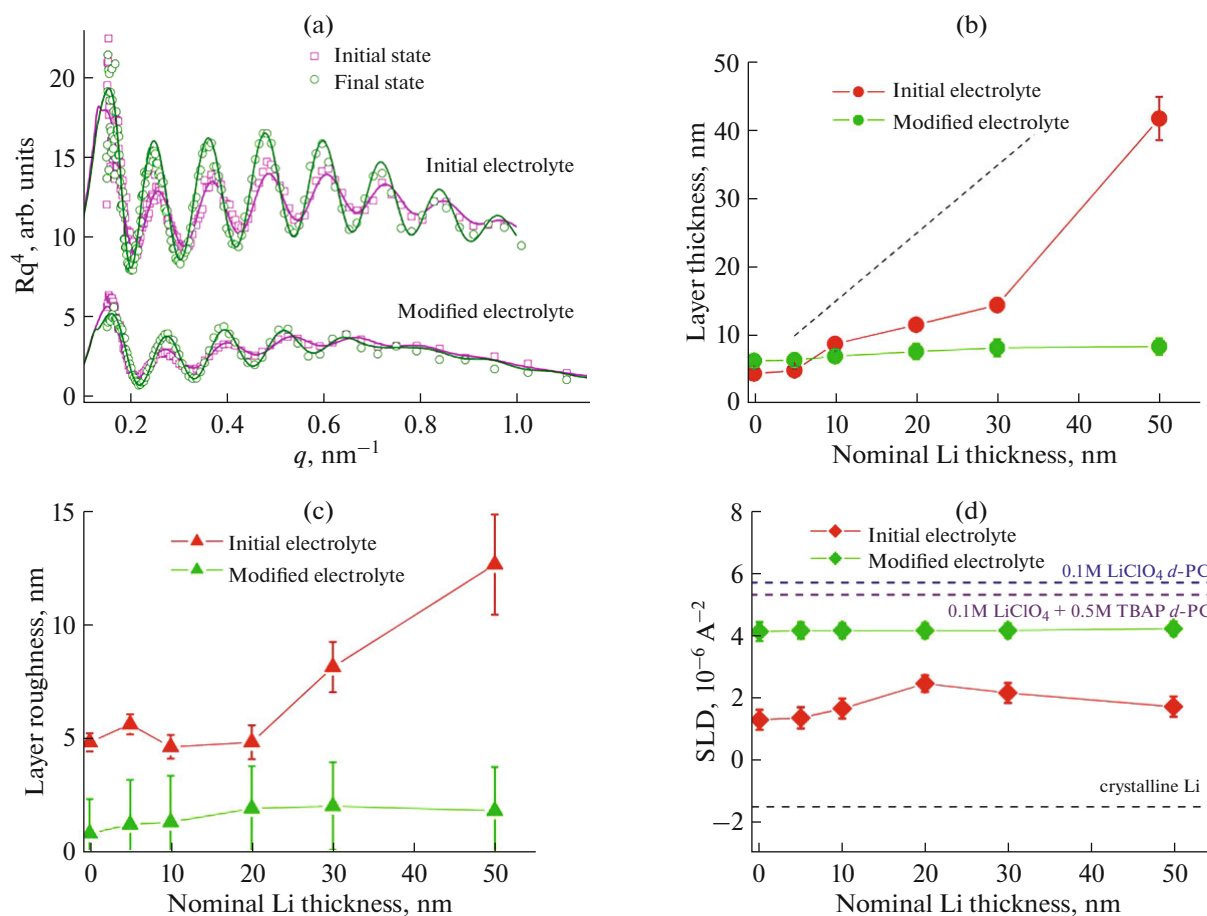


Fig. 10. (a) Experimental results (data points) and model (solid lines) curves of specular neutron reflection in the initial (zero charge) and final (maximum charge) states illustrating maximal effects for two types of electrolytes (standard electrolyte and electrolyte with nonelectroactive additive TBAP for suppressing growth of dendrites). Two groups of curves are shifted along the ordinate axis for visual convenience. Dependences of the deposited layer parameters on the total charge passed through the cell after the formation of the SEI, including layer thickness (a), layer roughness (b), and average SLD (c). The dashed line in (a) corresponds to the linear dependence implying uniform lithium deposition in the layer. Horizontal dashed lines in (c) show SLDs of crystalline Li and electrolytes for comparison with the SLD obtained for the layer. The experimental data are obtained using the GRAINS time-of-flight reflectometer at the JINR IBR-2 pulsed reactor (Dubna, Russia). The figure is reproduced by permission from [29] (©Elsevier, 2019).

scattering in the detector plane is isotropic and depends only on the magnitude of the scattering vector; a one-dimensional function—scattering curve—is analyzed, which is the Fourier transform of the pair correlation function for fluctuations of the SLD inside inhomogeneities relative to the SLD of the homogeneous medium that contains the inhomogeneities. At the uncorrelated arrangement of inhomogeneities in the medium (diluted systems) the scattering intensity is defined by the average form factor of the inhomogeneity. The average difference between the SLDs of the inhomogeneities and the medium determines the contrast. At the zero contrast scattering almost disappears because both inhomogeneities and the medium averagely scatter radiation despite a different chemical composition. If inhomogeneities are spherical multilayer particles, the problem of reconstructing the SLD profile in one particle is identical to the prob-

lem of specular neutron reflectometry. In both cases, the SLD profile is reconstructed in the neighborhood of the interface: in NR the SLD profile is the distance function of the initial density, and in SANS it is the function of the radius in a spherical particle counted from the particle center. Short-range order in the arrangement of inhomogeneities in the medium leads to additional modulation of the scattering intensity via the structural factor, the Fourier transform of the radial distribution function. Long-range order in the arrangement of inhomogeneities is described by the structural factor similar to the atomic structural factor in Bragg diffraction. This order causes formation of diffraction reflections with the q position inversely proportional to the repeatability period commensurate with the inhomogeneity size.

In fact, SANS is a variation of neutron transmission diffraction. However, the application of this

method to the *in situ/operando* studies of electrochemical assemblies is faced with more significant difficulties. While transmission diffraction in crystalline materials allows separation of contributions from components, which have well-separable diffraction peaks in diffraction patterns, this is not the case with small-angle diffraction, where because of nanosized inhomogeneities in their structure, all assembly components make a particular contribution to beam broadening, that is, actually to one peak. For this reason, a problem arises as to extraction of useful scattering caused by the assembly component under investigation. In some cases, this is obviated using the *ex situ* mode. With SANS, it is practically not very difficult. The component under study is transferred (in an airtight box) without any modifications from the laboratory electrochemical cell after its charge or discharge to a special hermetically sealed container with walls that weakly scatter and weakly absorb neutrons. Another difficulty is that electrode materials, separators, and especially solid electrolytes usually give rise to scattering most problematic to interpret, since they are multiphase systems with polydisperse formations and often with ill-defined internal interphase boundaries. In some cases, partial separation of information is achieved by using liquid electrolytes with different degrees of deuteration. Yet, the analysis mainly deals with integral characteristics (e.g., total scattering intensity or zero-angle scattering intensity), the evolution of which is ascribed to variations in electrochemical parameters. In one of the first works on this line of research [38], the SANS method was used to investigate anode materials for lithium-ion batteries on the basis of mesoporous materials, in particular carbon (ordered mesoporous carbon, OMC). The contrast distribution in the case of using a fully deuterated electrolyte allows relating variations in the scattering curve only to occurrence of lithium-containing deposition. Variations in scattering are associated with the potential variations during the discharge/charge cycle that lead to formation of the SEI on the internal surface of the pores. This approach was extended to various kinds of materials and liquid electrolytes in [39–41], where, in addition to formation of SEI, lithium intercalation and consequent broadening of the carbon framework for mesoporous carbon were detected. It is also tried to track SEI formation using SANS in more complex electrode materials. In [42], promising silicon-graphite (SiG) anodes were considered. Lithiation/delithiation observed during the cycling (up to 30 cycles) causes considerable morphological changes in silicon nanoparticles (size ~ 200 nm), which leads to formation of highly porous silicon structures and side reactions at the silicon/electrolyte interface. Quantitative estimation of these morphological changes was performed using selective contrasting of silicon nanoparticles and surrounding decomposition prod-

ucts of the electrolyte (1.5 mol/L LiPF₆ in EC). In addition, information on the SEI was obtained in *ex situ* experiments. After the first and last cycles, nanoparticles were also monitored using TEM. In [43], SANS was used to clarify the question of possible SEI formation at the surface of the Li₄Ti₅O₁₂ (LTO) cathode. The layer was assumed to form at cyclic switching of the cell. Cubic mesostructured LTO with the crystallite sizes of 3 to 4 nm and homogeneous pores ≤ 8 nm in diameter was synthesized for the investigations. The average pore size was adjusted between 4 and 8 nm using an amphiphathic triblock copolymer (with an adjustable hydrophobic block as a template) and thermal treatment. The LTO material was investigated by the SANS and XPS methods, which showed that the SEI under discussion formed at potentials of up to 2.2 V as a layer rich in LiF subsequently followed by growth of a carbon layer.

The SANS method is most effective for systems where structural features help increase informativeness of the experimental data. In cooperation with the Faculty of Chemistry of MSU, FLNP used a special approach to the application of SANS to study porous carbon electrodes in lithium–oxygen batteries [44]. It was found that discharge of such assemblies strongly depends on the type of the electrolyte used. To clarify microscopic aspects of the phenomenon, SANS experiments were carried out at the YuMO facility [45] of the IBR-2 reactor during the discharge of cells with two types of electrolytes (based on acetonitrile (MeCN) and dimethyl sulfoxide (DMSO)) and cathodes of standardized carbon paper with fixed thickness. With SANS, nanoformations of lithium-containing compounds are well seen when liquid electrolytes based on deuterated solvents are used (Fig. 11). The experiment was conducted in the *ex situ* mode. Difference curves (subtraction of residual scattering by closed pores) after discharge are appreciably different for two considered electrolytes and explain the difference in discharge from the microscopic point of view (Fig. 12). In the case of MeCN, we have heterogeneous passivation of the internal boundary in carbon grains with continuous blocking of oxygen diffusion paths in the grains. In the case of DMSO, passivation is close to homogeneous, since much of Li₂O₂ leaves the grains and is deposited in the intergrain space, additionally preventing oxygen from accessing the external surface of the grains. A consequence is a small diffraction peak observed at large q in the case of DMSO. This corresponds to ordered supramolecular structures of peroxide plates electron-microscopically observed on the external surface of the electrodes. In the case of MeCN, only nuclei of these structures are seen, which do not give a diffraction peak yet. Dependence of the results on the residual humidity (a few hundred ppm) of DMSO was observed. The conclusions are confirmed by the data of the SAXS/WAXS *operando* experiments [46].

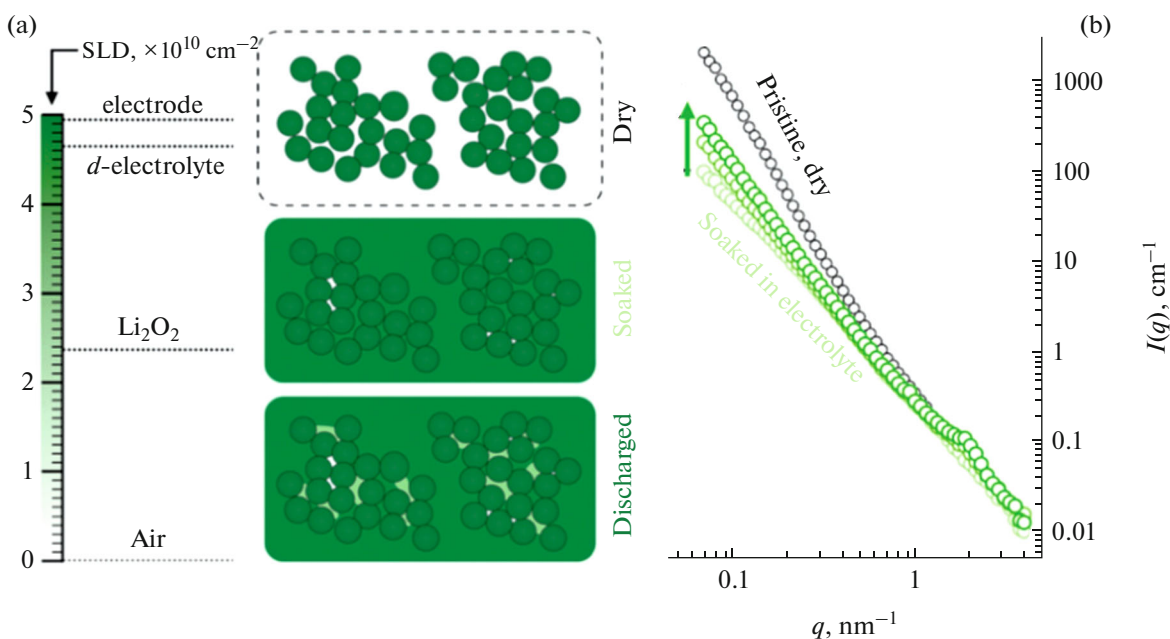


Fig. 11. (a) Pictorial diagram of the stages of the SANS experiment with porous carbon electrodes from model lithium–oxygen cells (top to bottom): the dry electrode, the main contribution to the scattering comes from open and closed pores; the undischarged electrode wetted with deuterated electrolyte, the main contribution to the scattering comes from closed pores; the discharged electrode wetted with the deuterated electrolyte, the main contribution to the scattering comes from closed pores and deposited lithium peroxide. (b) SANS curves for different stages of the experiment. Black and green correspond to the dry and wet electrodes, respectively. The green arrow shows the direction of the discharge. The electrolyte: 1 M LiTFSI DMSO-d₆. The experimental data are obtained using the GRAINS time-of-flight reflectometer at the JINR IBR-2 pulsed reactor (Dubna, Russia). The figure is reproduced from [44].

4. STRUCTURAL DIAGNOSTICS

By diagnostics are meant experiments that are conducted to obtain certain characteristics of materials in lithium storage devices, first of all for improving preparation of the final material or device. In some cases, division of investigations into exploratory and applied is arbitrary. Usually, the diagnostic experiment is aimed at achieving the maximum possible structural homogeneity of storage device components on different scales, stability in time, and as a consequence, the best electrochemical characteristics. Investigations of this kind are more applied in nature and can be commercialized. By and large, division of experiments into exploratory and diagnostic gives an idea of the trend in development of applications of synchrotron and neutron methods to investigations of lithium storage devices. Below are a few examples to illustrate the main directions of using synchrotron and neutron methods for diagnostic purposes.

Now the experience gained from the neutron-diffraction studies of electrodes in model electrochemical cells allows passing to more complicated commercial systems. While model cells are optimized to obtain high-statistics diffraction data from individual electrodes, in real systems the points of interest are structural transformations in both electrodes, in particular synchronous variations in the structure and phases of

the electrodes in the operating battery. Natural difficulties for these experiments are numerous impurity peaks in diffraction patterns and nonoptimal geometry of the sample, which leads to loss of useful information. Nevertheless, some characteristic diffraction reflections and their evolution during cycling can be detected and analyzed.

The first investigation of commercial cells at FLNP can be considered to be the above-described application of diffraction to prototypes of flat batteries with the LFP-based cathode (see Section 3.1.1). The success of that research motivated further development of neutron diffraction capabilities for studying the composition and structure of electrode materials (including those other than lithium iron phosphates) and the processes that occur during discharge/charge in the finished commercial items.

In [47], a type 18650 commercial cylindrical chargeable battery with a LiMO₂ cathode (M-transition metal) and a graphite counter electrode (Li_xC₆) was investigated without its any preliminary preparation for improvement of experimental conditions. These investigations demonstrated the capabilities of the IBR-2 reactor for neutron diffraction analysis of structural transformations in commercial lithium-ion rechargeable batteries during charge/discharge cycles. Its ex situ neutron diffraction pattern allowed identifying the type of the

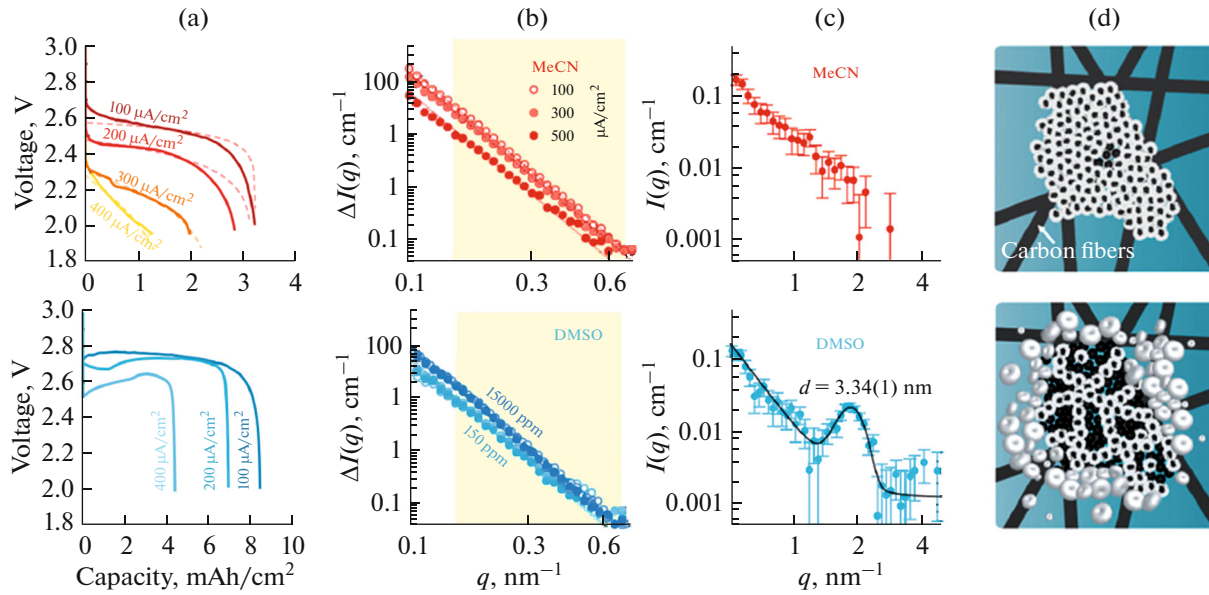


Fig. 12. Experimental data obtained at the lithium–oxygen model cells from different liquid electrolyte bases, acetonitrile MeCN (top row) and dimethyl sulfoxide DMSO (bottom row). (a) Voltage profile during discharge at different rates; (b) initial region of SANS curves after discharge at different rates; (c) final region of SANS curves after discharge at different rates; (d) pictorial view of the lithium peroxide deposition process in the carbon cathode. The experimental SANS curves are obtained using the YuMO facility at JINR IBR-2 reactor (Dubna, Russia). The figure is reproduced from [44].

cathode material ($\text{LiNi}_{1-x-y}\text{Co}_x\text{Mn}_y\text{O}_2$), and the accumulated operando diffraction spectra enabled real-time (diffraction pattern accumulation time 5 min) tracking of the structural transformation of cathode and anode materials in the course of three charge/discharge cycles at different rates. On the basis of the data obtained, the occurring intermediate phases were reliably identified, and kinetics of phase transformations in electrode materials was quantitatively analyzed. However, the cation content of the cathode formula unit ($\text{LiNi}_{0.5}\text{Co}_{0.2}\text{Mn}_{0.3}\text{O}_2$) could be determined more accurately only after the X-ray spectral elemental analysis, which required extraction of the cathode material from the battery. Neutron and X-ray diffraction of the extracted positive electrode powder made it possible to analyze diffraction peak profiles by the Warren–Averbach method and obtain the size distribution of the cathode crystallites corresponding to the log-normal distribution.

Further operando experiments with commercial batteries were conducted to investigate phase stability of another cathode material, $\text{LiNi}_{0.8}\text{Co}_{0.15}\text{Al}_{0.05}\text{O}_2$ (NCA) [48]. To this end, experiments were performed with type 18650 cylindrical cells with the NCA and graphite electrodes. Dependence of structural phases of the anode on the battery charge/discharge rate was quantitatively determined from the measured diffraction patterns (time resolution 75 s) (Fig. 13). No phase layering of the cathode material was found in the entire investigated current range (from 0.1 to 0.5C), which is a positive characteristic for these systems.

Additionally, quantitative relation between the fraction of the anode material passing into the charged state and the battery charge rate was determined, and different kinetics was observed for lithium intercalation/deintercalation to graphite. This difference is due to the inhomogeneous distribution of lithium in the anode material, both over the cell as a whole and inside the graphite particles. Nonlinear dependences of parameters of the elementary cell, interplanar and interlayer distances on the lithium content of the cathode were obtained, which is caused by several factors, such as variation in the degree of oxidation of the cation in oxygen octahedrons, Coulomb repulsion and change of the average effective charge of oxygen layers, and Van der Waals interaction between MeO_2 layers at a high level of NCA delithiation. Qualitative agreement was established between the experimental results and the results of model calculations from first principles [49, 50].

The problem of structural homogeneity concerns all components of storage devices, beginning with electrode materials. Homogeneity of cathode materials was investigated at FLNP in cooperation with the Dubna State University, Institute of Nuclear Physics (Ministry of Energy of the Republic of Kazakhstan), and Faculty of Physics of Kyiv National University. Figure 14 shows an example of applying SANS to the cathode material with conductive carbon additives [51]. The SANS experiments were conducted in addition to electron microscopy for LFP cathodes filled with the standard C45 carbon black additive and the carbon nanotube (CNT) additive under investigation.

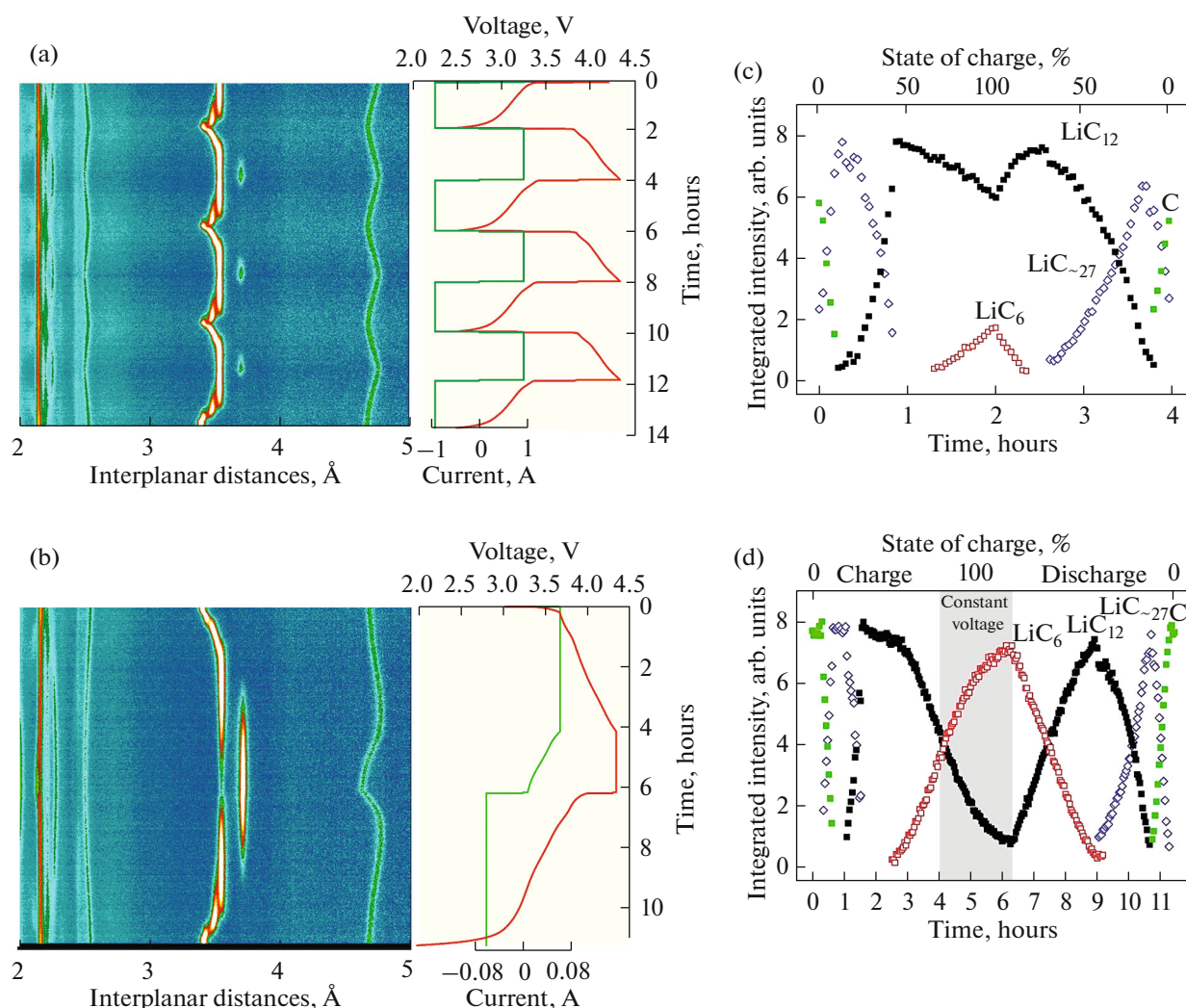


Fig. 13. Evolution of NPD diffraction patterns during the cell charge/discharge at different rates, C/3 (a) and C/5 + constant voltage (CV) (b). The intense diffraction peaks at $d = 3.4\text{--}3.7$ Å correspond to Li_xC_6 phases. The diffraction peak at $d \approx 4.7$ Å is the (003) reflection of the cathode material. Evolutions of the graphite phase content proportional to the intensity of the corresponding diffraction reflections are shown for one cycle with the rate C/3 (c) and C/5 + constant voltage (CV) (d). The battery charge/discharge rate is seen to govern the number of the anode phases and the phase formation kinetics. The NPD data are obtained using the RTD time-of-flight diffractometer at the JINR IBR-2 reactor (Dubna, Russia). The figure is reproduced by permission from [48] (©Elsevier, 2021).

Analysis of closed/open porosity was performed using wetting with deuterated electrolyte to compensate scattering from open pores. A change in scattering for dry and wet samples depends on the type of additive and its content. With CNTs, considerable decrease in the scattering was observed for both dry and wet samples. This means that CNTs effectively mix with the LFP matrix and fill the intergrain space, which significantly improves liquid electrolyte accessibility. As a consequence, electrodes with 1% of CNTs demonstrate higher specific capacity as compared to electrodes with 5–15% of carbon black. It was shown that CNTs as a conductive additive open up a possibility of manufacturing electrodes with a capacity higher than 5 mA h cm^{-2} . Practical applicability of the considered

electrode technology is confirmed on the basis of the prototype coffee bag element with the specific energy density of 150 W h/kg , 295 W h/L .

The current trend is to use lithium storage devices with solid electrolytes, which generally ensure higher operational and ecological safety than storage devices with liquid electrolytes. Many types of solid electrolytes have been developed that exhibit competitive ion conduction compared to liquid electrolytes [52, 53]. These are glasses and glass-ceramics (e.g., $\text{Li}_6\text{PS}_5\text{Cl}$), isostructural compounds (e.g., $\text{Li}_{14}\text{Zn}(\text{GeO}_4)_4/\text{Li}_{4-x}\text{Ge}_{1-x}\text{P}_x\text{S}_4$) and their analogs, and oxides of the NASICON and garnet types. Mobility of the Li^+ cation in them is ensured, as in macrocrystalline materials, by hopping conduction between lattice interstitial sites. However, develop-

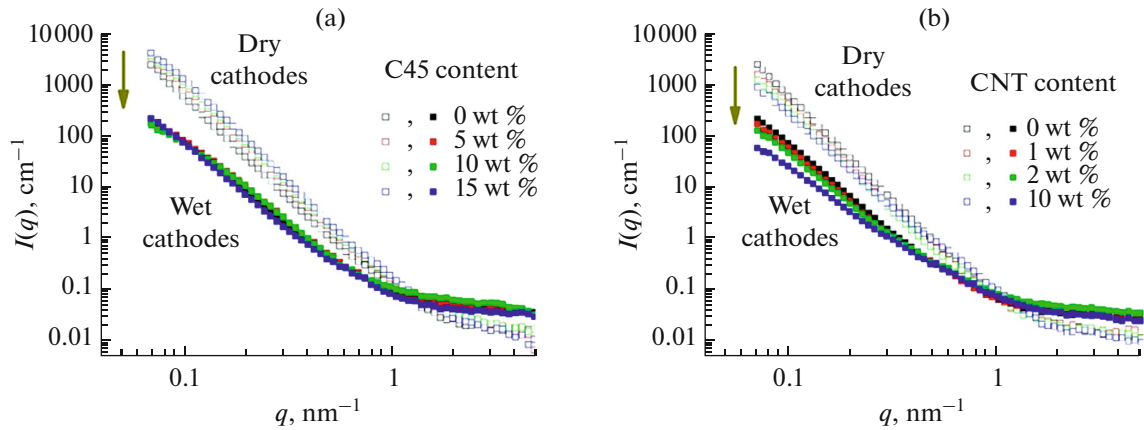


Fig. 14. Curves of SANS on cathodes for LFP-based lithium-ion storage devices of the intercalation type with two kinds of conductive additive, carbon C45 (a) and carbon nanotubes CNTs (b). The measurements are made for dry cathodes and cathodes wetted with the deuterated liquid electrolyte base (LiTFSI). Different changes in curves of two types with increasing additive concentration indicate different packing of carbon additives in the intergrain space. Experimental SANS curves are obtained using the YuMO facility at the JINR IBR-2 reactor (Dubna, Russia). The data are taken from [51].

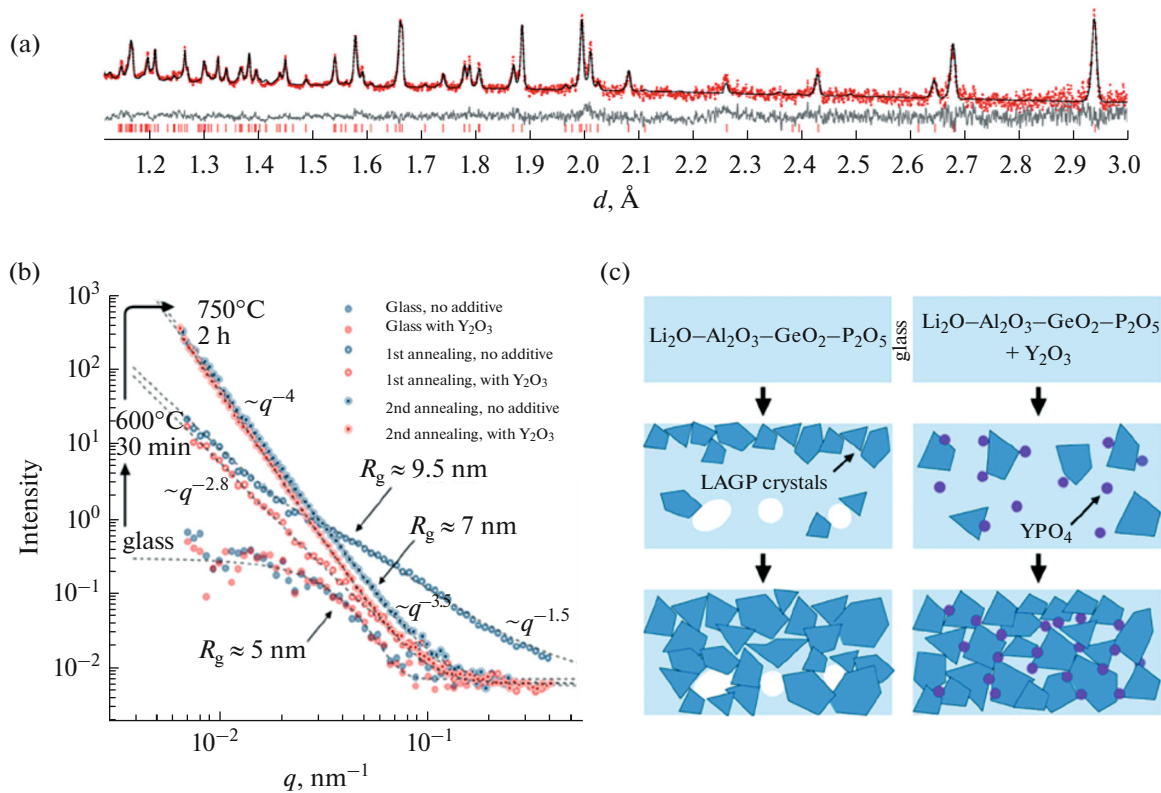


Fig. 15. (a) Diffraction patterns for the LAGP glass-ceramic before and after double annealing of the initial glass. The LAGP peaks indicate bulk crystallization. The experimental diffraction patterns are obtained using the HRFD facility at the JINR IBR-2 reactor (Dubna, Russia). (b) SANS on LAGP at different synthesis stages, including initial glass (scattering by pores), after the first and second annealing for crystallization of pure LAGP, and with addition of Y_2O_3 to the initial composition. The experimental SANS curves are obtained using the YuMO facility at the JINR IBR-2 reactor (Dubna, Russia). (c) Pictorial view of the structure evolution from the neutron scattering data for pure LAGP and with Y_2O_3 added. The figure is reproduced from [54].

ment of the most uniform and homogeneous possible structure of these electrolytes requires special protocols. For example, glass-ceramics are produced by two- or three-stage annealing of the initial glass at the

temperature above the glass transition point. The reason for using a complicated process is that annealing by external heating causes heterogeneous nucleation: the forming crystal grains are strongly nonspherical in

shape, they are nonuniformly distributed in the material, and many pores develop. As a result, materials have low ion conduction and poor mechanical properties. To homogenize the final structure, various additives are added to glass.

At FLNP, together with the Faculty of Chemistry of MSU, an integrated structural analysis of glass-ceramic solid electrolytes was carried out using diffraction and SANS for improving their synthesis [54, 55]. Promising solid electrolytes $\text{Li}_{1-x}\text{Al}_x\text{Ge}_{2-x}(\text{PO}_4)_3$ (LAGP, NASICON structure) with Y additives were studied. Figure 15 shows the results of this investigation. High-resolution neutron diffraction was successfully used to investigate the degree of crystallization and the crystal structure. The LAGP ceramic materials with different crystallization time doped and not doped with Y_2O_3 were investigated. Samples for the neutron diffraction experiment were powdered. The ensuing data allowed establishing the presence and quantity of impurity phases, refining parameters of the crystal structure, and showing that population of lithium positions in the LAGP structure depended on the electrolyte crystallization time and achieved the maximum in two hours of annealing in the air at 750°C . Phase homogeneity was efficiently monitored by SANS. Modification by adding an yttrium compound as a homogenizer led to increasing ion conduction (up to a factor of five). Crystallization by double annealing shows difference in phase formation without and with addition of an yttrium compound. The increase in conduction results from the increase in the number of contact points of crystalline grains.

6. CONCLUSIONS

The presented neutron investigations fully reflect the fact that the IBR-2 pulsed reactor of FLNP (JINR, Dubna, Russia) meets the demands of modern electrochemistry, in particular regarding structure investigations and diagnostics of electrode materials and electrochemical interfaces. Actually, a specialized infrastructure for electrochemical investigations is built at the IBR-2, and its efficiency is confirmed by experiments with lithium energy storage devices.

The penetrating nature of neutron radiation and availability of such a high-intensity neutron source as the IBR-2 make it possible to investigate the hidden microstructure of materials and physicochemical processes in lithium storage devices at a new level. In many cases, systems are studied under conditions close to reality in real time, which determines a transition from the study of equilibrium processes to the study of nonequilibrium processes. Apart from classical approaches related to crystalline materials, methods referring to nanostructured materials are being actively devised at the IBR-2 that help improve characteristics of lithium-ion batteries and develop new classes of storage devices. Also, neutron scattering

methods allows tracking occurrence and growth of structural inhomogeneities in components of lithium batteries, which makes it possible to solve problems of their optimization concerning higher energy capacity, longer service life, and ensured operational safety.

ACKNOWLEDGMENTS

The part of the review dealing with diffraction methods of research was supported by the Russian Science Foundation, project no. 21-12-00261.

REFERENCES

1. A. M. Balagurov, I. A. Bobrikov, N. Y. Samoylova, O. A. Drozhzhin, and E. V. Antipov, "Neutron scattering for analysis of processes in lithium-ion batteries," *Rus. Chem. Rev.* **83**, 1120–1134 (2014).
2. D. M. Itkis, J. J. Velasco-Velez, A. Knop-Gericke, A. Vyalikh, M. V. Avdeev, and L. V. Yashina, "Probing of electrochemical interfaces by photons and neutrons in operando," *ChemElectroChem* **2**, 1427–1445 (2015).
3. M. V. Avdeev, I. A. Bobrikov, and V. I. Petrenko, "Neutron methods for tracking lithium in operating electrodes and interfaces," *Phys. Sci. Rev.* **3**, 20170157 (2018).
4. H. Zhu, Y. Huang, H. Zhu, L. Wang, S. Lan, X. Xia, and Q. Liu, "In situ probing multiple-scale structures of energy materials for Li-ion batteries," *Small Methods* **4**, 1900223 (2019).
5. D. Liu, Z. Shadik, R. Lin, K. Qian, H. Li, K. Li, S. Wang, Q. Yu, M. Liu, S. Ganapathy, X. Qin, Q.-H. Yang, M. Wagemaker, F. Kang, X.-Q. Yang, and B. Li, "Review of recent development of in situ/operando characterization techniques for lithium battery research," *Adv. Mater.* **31**, 1806620 (2019).
6. E. Zhao, Z.-G. Zhang, X. Li, L. He, X. Yu, H. Li, and F. Wang, "Neutron-based characterization techniques for lithium-ion battery research," *Chinese Phys. B* **29**, 018201 (2020).
7. K. Xu, "Nonaqueous liquid electrolytes for lithium-based rechargeable batteries," *Chem. Rev.* **104**, 4303–4417 (2004).
8. T. Placke, R. Kloepsch, S. Dühnen, and M. Winter, "Lithium ion, lithium metal, and alternative rechargeable battery technologies: The odyssey for high energy density," *J. Solid State Electrochem.* **21**, 1939–1964 (2017).
9. A. A. Rulev, A. V. Sergeev, L. V. Yashina, T. Jacob, and D. M. Itkis, "Electromigration in lithium whisker formation plays insignificant role during electroplating," *ChemElectroChem* **6**, 1324–1328 (2019).
10. J. M. Tarascon and M. Armand, "Issues and challenges facing rechargeable lithium batteries," *Nature* **414**, 359–367 (2001).
11. W. Xu, J. Wang, F. Ding, X. Chen, E. Nasybulin, Y. Zhang, and Ji-G. Zhang, "Lithium metal anodes for rechargeable batteries," *Energy Environ. Sci.* **7**, 513–537 (2014).

12. Y. Zhang, Y. Zhao, K. E. Sun, and P. Chen, "Development in lithium/sulfur secondary batteries," *Open Mater. Sci. J.* **5**, 215–221 (2011).
13. J. Yamaki, S. Tobishima, K. Hayashi, K. Saito, Y. Nemoto, and M. Arakawa, "A consideration of the morphology of electrochemically deposited lithium in an organic electrolyte," *J. Power Sources* **74**, 219–227 (1998).
14. J. Steiger, G. Richter, M. Wenk, D. Kramer, and R. Mönig, "Comparison of the growth of lithium filaments and dendrites under different conditions," *Electrochem. Commun.* **50**, 11–14 (2015).
15. A. M. Balagurov, I. A. Bobrikov, G. D. Bokuchava, V. V. Zhuravlev, and V. G. Simkin, "Correlation Fourier diffraction: 20 years of experience at the IBR-2 reactor," *Phys. Part. Nucl.* **46**, 249–276 (2015).
16. A. M. Balagurov, A. I. Beskrovnyy, V. V. Zhuravlev, G. M. Mironova, I. A. Bobrikov, D. Neov, and S. G. Sheverev, "Neutron diffractometer for real-time studies of transient processes at the IBR-2 pulsed reactor," *J. Surf. Invest.* **10**, 467–479 (2016).
17. I. A. Bobrikov, A. M. Balagurov, C.-W. Hu, C.-H. Lee, S. Deleg, and D. A. Balagurov, "Structural evolution in LiFePO₄-based battery materials: In-situ and ex-situ time-of-flight neutron diffraction study," *J. Power Sources* **258**, 356–364 (2014).
18. N. V. Kosova, I. A. Bobrikov, O. A. Podgornova, A. M. Balagurov, and A. K. Gutakovskii, "Peculiarities of structure, morphology, and electrochemistry of the doped 5-V spinel cathode materials LiNi_{0.5-x}Mn_{1.5-y}M_x+yO₄ (M = Co, Cr, Ti; X + Y = 0.05) prepared by mechanochemical way," *J. Solid State Electrochem.* **20**, 235–246 (2016).
19. E. A. Sherstobitova, A. F. Gubkin, I. A. Bobrikov, A. V. Kalashnova, and M. I. Pantyukhina, "Bottlenecked ionic transport in Li₂ZrO₃: High temperature neutron diffraction and impedance spectroscopy," *Electrochim. Acta* **209**, 574–581 (2016).
20. N. Sharma, W. K. Pang, Z. P. Guo, and V. K. Peterson, "In situ powder diffraction studies of electrode materials in rechargeable batteries," *ChemSusChem* **8**, 2826–2853 (2015).
21. I. A. Bobrikov, N. Yu. Samoylova, O. Yu. Ivanshina, R. N. Vasin, S. V. Sumnikov, E. A. Kornieieva, and A. M. Balagurov, "Abnormal phase-separated state of LiNi_{0.8}Co_{0.15}Al_{0.05}O₂ in the first charge: Effect of electrode compaction," *Electrochim. Acta* **265**, 726–735 (2018).
22. Y. Lauw, T. Rodopoulos, M. Gross, A. Nelson, R. Gardner, and M. D. Horne, "Electrochemical cell for neutron reflectometry studies of the structure of ionic liquids at electrified interface," *Rev. Sci. Instrum.* **81**, 074101 (2010).
23. B. Jerliu, L. Dörrer, E. Hüger, G. Borchardt, R. Steitz, U. Geckle, V. Oberst, M. Bruns, O. Schneider, and H. Schmidt, "Neutron reflectometry studies on the lithiation of amorphous silicon electrodes in lithium-ion batteries," *Phys. Chem. Chem. Phys.* **15**, 7777–7784 (2013).
24. M. Yonemura, M. Hirayama, K. Suzuki, R. Kanno, N. Torikai, and N. L. Yamada, "Development of spectroelectrochemical cells for in situ neutron reflectometry," *J. Phys. Conf. Ser.* **502**, 012054 (2014).
25. S. C. DeCaluwe, B. M. Dhar, L. Huang, Y. He, K. Yang, J. P. Owejan, Y. Zhao, A. A. Talin, J. A. Dura, and H. Wang, "Pore collapse and regrowth in silicon electrodes for rechargeable batteries," *Phys. Chem. Chem. Phys.* **17**, 11301–11312 (2015).
26. H. Kawaura, M. Harada, Y. Kondo, H. Kondo, Y. Sukanuma, N. Takahashi, J. Sugiyama, Y. Seno, and N. L. Yamada, "Operando measurement of solid electrolyte interphase formation at working electrode of Li-ion battery by time-slicing neutron reflectometry," *ACS Appl. Mater. Interfaces* **8**, 9540–9544 (2016).
27. M. V. Avdeev, A. A. Rulev, V. I. Bodnarchuk, E. E. Ushakova, V. I. Petrenko, I. V. Gapon, O. V. Tomchuk, V. A. Matveev, N. K. Pleshanov, E. Yu. Kataev, L. V. Yashina, and D. M. Itkis, "Monitoring of lithium plating by neutron reflectometry," *Appl. Surf. Sci.* **424**, 378–382 (2017).
28. C. H. Lee, J. A. Dura, A. LeBar, and S. C. DeCaluwe, "Direct, operando observation of the bilayer solid electrolyte interphase structure: Electrolyte reduction on a non-intercalating electrode," *J. Power Sources* **412**, 725–735 (2019).
29. A. Ronneburg, "Surface structure inhibited lithiation of crystalline silicon probed with operando neutron reflectivity," *Energy Storage Mater.* **18**, 182–189 (2019).
30. E. D. Rus and J. A. Dura, "In situ neutron reflectometry study of solid electrolyte interface (SEI) formation on tungsten thin-film electrodes," *ACS Appl. Mater. Interfaces* **11**, 47553–47563 (2019).
31. J. A. Dura, E. D. Rus, P. A. Kienzle, and B. B. Maranville, "Nanolayer analysis by neutron reflectometry," in *Nanolayer Research* (Elsevier, 2017), pp. 155–202.
32. J. E. Owejan, J. P. Owejan, S. C. DeCaluwe, and J. A. Dura, "Solid electrolyte interphase in Li-ion batteries: Evolving structures measured in situ by neutron reflectometry," *Chem. Mater.* **24**, 2133–2140 (2012).
33. M. V. Avdeev, V. I. Bodnarchuk, V. I. Petrenko, I. V. Gapon, O. V. Tomchuk, A. V. Nagorny, V. A. Ulyanov, L. A. Bulavin, and V. L. Aksenov, "Neutron time-of-flight reflectometer GRAINS with horizontal sample plane at the IBR-2 reactor: Possibilities and prospects," *Cryst. Rep.* **62**, 1002–1008 (2017).
34. V. I. Petrenko, Ye. N. Kosiachkin, L. A. Bulavin, and M. V. Avdeev, "Optimization of the initial interface configuration for in-situ neutron reflectometry experiments," *J. Surf. Invest.* **14**, 215–219 (2020).
35. V. I. Petrenko, Ye. N. Kosiachkin, L. A. Bulavin, and M. V. Avdeev, "On enhancement of the adsorption-layer effect at the metallic electrode-liquid electrolyte interface in specular neutron reflectometry experiments," *J. Surf. Invest.* **12**, 651–657 (2018).
36. M. V. Avdeev, A. A. Rulev, E. E. Ushakova, Ye. N. Kosiachkin, V. I. Petrenko, I. V. Gapon, E. Yu. Kataev, V. A. Matveev, L. V. Yashina, and D. M. Itkis, "On nanoscale structure of planar electrochemical interfaces metal/liquid lithium ion electrolyte by neutron reflectometry," *Appl. Surf. Sci.* **486**, 287–291 (2019).
37. E. Yu. Kataev, I. V. Gapon, D. M. Itkis, A. I. Belova, and M. V. Avdeev, RF Patent No. 2654317 (2018).

38. C. A. Bridges, X.-G. Sun, J. Zhao, M. P. Paranthaman, and S. Dai, "In situ observation of solid electrolyte interphase formation in ordered mesoporous hard carbon by small-angle neutron scattering," *J. Phys. Chem. C* **116**, 7701–7711 (2012).
39. R. L. Sacci, J. Bañuelos, J. Leobardo, G. M. Veith, K. C. Littrell, Y. Q. Cheng, C. U. Wildgruber, L. L. Jones, A. J. Ramirez-Cuesta, G. Rother, and N. J. Dudney, "Structure of spontaneously formed solid-electrolyte interphase on lithiated graphite determined using small-angle neutron scattering," *J. Phys. Chem. C* **119**, 9816–9823 (2015).
40. C. A. Bridges, X.-G. Sun, B. Guo, L. He, and S. Dai, "Observing framework expansion of ordered mesoporous hard carbon anodes with ionic liquid electrolytes via in situ small-angle neutron scattering," *ACS Energy Lett.* **2**, 1698–1704 (2017).
41. C. J. Jafta, X.-G. Sun, G. M. Veith, G. V. Jensen, S. M. Mahurin, M. P. Paranthaman, S. Dai, and C. A. Bridges, "Probing microstructure and electrolyte concentration dependent cell chemistry via operando small angle neutron scattering," *Energy Environ. Sci.* **12**, 1866–1877 (2019).
42. N. Paul, M. Wetjen, S. Busch, H. Gasteiger, and R. Gilles, "Contrast matched SANS for observing SEI and pore clogging in silicon-graphite anodes," *J. Electrochem. Soc.* **166**, A1051–A1054 (2019).
43. C. J. Jafta, C. A. Bridges, Y. Bai, L. Geng, B. P. Thapaliya, H. M. Meyer, R. Esselhi, W. T. Heller, and I. Belharouak, "Probing the $\text{Li}_4\text{Ti}_5\text{O}_{12}$ interface upon lithium uptake by operando small angle neutron scattering," *ChemSusChem* **13**, 3654–3661 (2020).
44. T. K. Zakharchenko, M. V. Avdeev, A. V. Sergeev, A. V. Chertovich, O. I. Ivankov, V. I. Petrenko, Y. Shao-Horn, L. V. Yashina, and D. M. Itkis, "Small-angle neutron scattering studies of pore filling in carbon electrodes: Mechanisms limiting lithium-air battery capacity," *Nanoscale* **11**, 6838–6845 (2019).
45. A. I. Kuklin, O. I. Ivankov, A. V. Rogachev, D. V. Soloviov, A. K. Islamov, V. V. Skoi, Y. S. Kovalev, A. V. Vlasov, Y. L. Rzykai, A. G. Soloviev, N. Kucerkova, and V. I. Gordeliy, "Small-angle neutron scattering at the pulsed reactor IBR-2: Current status and prospects," *Cryst. Rep.* **66**, 231–241 (2021).
46. T. K. Zakharchenko, A. V. Sergeev, A. D. Bashkurov, P. Neklyudova, A. Cervellino, D. M. Itkis, and L. V. Yashina, "Homogeneous nucleation of Li_2O_2 under Li-O_2 battery discharge," *Nanoscale* **12**, 4591–4601 (2020).
47. I. A. Bobrikov, N. Yu. Samoylova, D. A. Balagurov, O. Yu. Ivanshina, O. A. Drozhzhin, and A. M. Balagurov, "Neutron diffraction analysis of structural transformations in lithium-ion batteries," *Rus. J. Electrochem.* **53**, 178–186 (2017).
48. I. A. Bobrikov, N. Yu. Samoylova, S. V. Sumnikov, O. Yu. Ivanshina, R. N. Vasin, A. I. Beskrovnyi, and A. M. Balagurov, "In-situ time-of-flight neutron diffraction study of the structure evolution of electrode materials in a commercial battery with $\text{LiNi}_{0.8}\text{Co}_{0.15}\text{Al}_{0.05}\text{O}_2$ cathode," *J. Power Sources* **372**, 74–81 (2017).
49. R. Eremin, P. Zolotarev, O. Yu. Ivanshina, and I. A. Bobrikov, "Li(Ni,Co,Al) O_2 cathode delithiation: A combination of topological analysis, density functional theory, neutron diffraction, and machine learning techniques," *J. Phys. Chem. C* **121**, 28293–28305 (2017).
50. R. Eremin, P. Zolotarev, and I. Bobrikov, "Delithiated states of layered cathode materials: Doping and dispersion interaction effects on the structure," *EPJ Web Conf.* **177**, 02001 (2018).
51. P. Napolskiy, M. V. Avdeev, M. S. Yerdautov, O. I. Ivankov, S. Bocharova, S. Ryzhenkova, B. Kaparova, K. Mironovich, D. Burlyayev, and V. A. Krivchenko, "On the use of carbon nanotubes in prototyping the high energy density Li-ion batteries," *Energy Technol.* **8**, 2000146 (2020).
52. C. Suna, J. Liub, Y. Gong, D. P. Wilkinsone, and J. Zhang, "Recent advances in all-solid-state rechargeable lithium batteries," *Nano Energy* **33**, 363–386 (2017).
53. F. Zheng, M. Kotobuki, S. Song, M. O. Lai, and L. Lu, "Review on solid electrolytes for all-solid-state lithium-ion batteries," *J. Power Sources* **389**, 198–213 (2018).
54. V. A. Vizgalov, T. Nestler, L. A. Trusov, I. A. Bobrikov, O. I. Ivankov, M. V. Avdeev, A. Vyalikh, D. C. Meyer, and D. M. Itkis, "Enhancing lithium-ion conductivity in NASICON glass-ceramics by adding yttria," *CrystEngComm* **20**, 1375–1382 (2018).
55. V. A. Vizgalov, T. Nestler, A. Vyalikh, I. A. Bobrikov, O. I. Ivankov, V. Petrenko, M. V. Avdeev, L. V. Yashina, and D. M. Itkis, "The role of glass crystallization processes in preparation of high Li-conductive NASICON-type ceramics," *CrystEngComm* **21**, 3106–3115 (2019).

Translated by M. Potapov